STUDIES IN MICROWAVE SPECTROSCOPY:

1. DIPOLE MOMENT OF GLYCIDALDEHYDE

2. ROTATIONAL RELAXATION IN CARBONYL SULFIDE AND AMMONIA

Thesis for the Degree of Ph. D.
MICHIGAN STATE UNIVERSITY
PERRY JOHN MANOR
1972

This is to certify that the

thesis entitled
STUDIES IN MICROWAVE SPECTROSCOPY
1. DIPOLE MOMENT OF GLYCIDALDEHYDE
2. ROTATIONAL RELAXATION IN CARBONYL SULFIDE AND AMMONIA

presented by

Perry John Manor

has been accepted towards fulfillment
of the requirements for

Ph.D. degree in Chemistry

R. F. Schwendeman

Major professor

Date February 9, 1972

O-7639

ABSTRACT

STUDIES IN MICROWAVE SPECTROSCOPY
1. DIPOLE MOMENT OF GLYCIDALDEHYDE
2. ROTATIONAL RELAXATION IN CARBONYL SULFIDE AND AMMONIA

By

Perry John Manor

Part 1.

A short history of microwave spectroscopy is presented. A brief discussion of the theory of the rigid rotor and the Stark effect is given. A description of the microwave spectrometer is presented together with a scheme for relative intensity measurements.

The microwave spectrum of trans-glycidaldehyde in the ground and first three excited torsional states was investigated. Three rotational constants were obtained for all states except for the third excited state where only B and C could be determined. The excited states were attributed to the aldehyde torsion, and the torsional excitation energy was estimated. The dipole moments of trans-glycidaldehyde were determined to be μ_a = 1.932 ± 0.005D, μ_b = 1.511 ± 0.017D, μ_c = 0.277 ± 0.156D, μ_T = 2.469 ± 0.031D. All attempts at locating transitions which could be attributed to the presence of another species were unsuccessful.

Part 2.

A brief review of important historic investigations which contributed to the understanding of line-shapes and line-broadening phenomena in the rotational spectroscopy of gases is given. A detailed investigation of

the ab

dent

paris

exper

radia

relax

mined

tions

to re

obtai

obtai

theor

is ac

level

many

width

is ab

molec

doubl

trans

radia

width

the absorption coefficient as a function of time for moderate power incident radiation which gives rise to partial saturation is given. A comparison of the theoretical expression for the absorption coefficient and experimental measurements for times a short time after the onset of the radiation provides an estimate of the pressure-dependent rotational relaxation rate constant.

The pressure dependent rotational relaxation rate constant is determined for the OCS J = 0 → 1, OCS J = 1 → 2, and the NH_3 J,K = 3,3 transitions under conditions of partial saturation and the results are compared to results obtained previously by linewidth measurements.

The linewidths of the OCS J = 0 → 1 and the OCS J = 1 → 2 transitions obtained from the relaxation studies are essentially the same as those obtained from previous linewidth measurements. According to relaxation theory, this would indicate that the mechanism for relaxation in OCS is accomplished primarily through energy transfer from the two energy levels which are in resonance with the radiation to one or more of the many other closely spaced rotational energy levels present. The linewidth obtained for the NH_3 J,K = 3,3 transition from relaxation studies is about 20 percent larger than that found previously. In the NH_3 molecule the energy levels are composed of widely spaced inversion doublets and therefore the relaxation must depend largely on energy transfer between the energy levels which are in resonance with the radiation. Under these conditions, relaxation theory predicts a linewidth that is twice that obtained from normal linewidth measurements.

STUDIES IN MICROWAVE SPECTROSCOPY:

1. DIPOLE MOMENT OF GLYCIDALDEHYDE

2. ROTATIONAL RELAXATION IN CARBONYL SULFIDE AND AMMONIA

by

Perry John Manor

A THESIS

Submitted to
Michigan State University
in partial fulfillment of the requirements
for the degree of

DOCTOR OF PHILOSOPHY

Department of Chemistry

1972

To Vranna for her constant encouragement and for her contribution through the typing of this manuscript.

Schw

gati

ackn

for p

Boxc

ACKNOWLEDGMENTS

I wish to extend a most sincere "thank you" to Professor Richard H. Schwendeman for his close supervision and help throughout these investigations and during the preparation of this thesis.

Financial support from the National Science Foundation is gratefully acknowledged.

Appreciation is extended to Princeton Applied Research Corporation for permission to reproduce Figure III-1 on page III-3 of their Model 160 Boxcar Integrator Manual.

TABLE OF CONTENTS

PART 1: DIPOLE MOMENT OF GLYCIDALDEHYDE

TABLE OF CONTENTS

PART 2: ROTATIONAL RELAXATION IN CARBONYL SULFIDE AND AMMONIA

TABL

I.

II.

III.

IV.

V.

VI.

VII.

VIII.

IX.

X.

XI.

LIST OF TABLES

LIST OF FIGURES

LIST OF FIGURES--continued

FIGURE Page

PART 1: DIPOLE MOMENT OF GLYCIDALDEHYDE

I. INTRODUCTION

Microwave spectroscopy concerns itself chiefly with the absorption of electromagnetic radiation which changes the rotation energy of molecules. Two requirements must be met by any molecule before its rotational spectrum can be studied by microwave spectroscopy: (1) it must have a reasonable vapor pressure at some convenient temperature and (2) it must possess a permanent dipole moment. The gas phase study of polar molecules is not necessarily limited to rotational motion alone since it is not possible to completely divorce this motion from that of vibrations or internal rotations within the molecule. Hence, it is necessary to use a theory which includes the particular interactions which affect the experimental spectra.

In 1933, at about the time Nielsen (1) introduced his theory of hindered internal rotation, which was later to be so important to this area of study, the first successful microwave experiment was carried out by Cleeton and Williams (2) who succeeded in producing the first experimentally obtained microwave spectrum when they observed a transition between a pair of the inversion levels of the ammonia molecule. However, prior to the mid-1940s microwave spectroscopy was principally a theoretical area of science and experimental techniques developed slowly until World War II, during which time radar was developed. This produced both the electronic knowledge and the equipment capable of doing the precision work necessary to generate the detailed spectra which the

th

in

an

th

sp

mo

an

wi

Eu

Sta

a m

mea

aut

to

men

cal

rota

rota

kind

spec

tati

spec

para

theory called for.

In 1946 Bleaney and Penrose (3) and Coles and Good (4) succeeded in producing the first high resolution spectra of the inversion in ammonia. At about the same time Dakin, Good, and Coles (5,6) observed the rotational Stark effect in the carbonyl sulfide molecule.

Probably one of the most significant contributions to microwave spectroscopy came when Hughes and Wilson (7) developed the first Stark-modulated spectrometer. Stark modulation coupled with the lock-in amplifier suggested by Michaels and Curtis (8) resulted in a spectrometer with greatly improved signal to noise ratio. A modification of the Hughes-Wilson spectrometer suggested by Karplus substituted square wave Stark modulation for the originally used sine wave form. This provided a more easily interpreted Stark effect and hence easier observation and measurement of the Stark splitting. Other important ideas such as automatic sweeping and stabilization techniques (9) have also helped to bring microwave spectroscopy to its present high level of advancement.

Today, microwave spectroscopy is capable of treating, both theoretically and experimentally, complex problems dealing with rotational motion, rotation-vibration interaction, Stark effect, dipole moments, internal rotation, quadrupole coupling, and molecular structure of many different kinds of polar molecules in the gaseous state. In addition, microwave spectroscopy is proving to be a highly valuable tool in both the qualitative and quantitative analysis of chemical compounds.

Part One of this thesis is concerned with the use of microwave spectroscopy to determine the dipole moment, Stark effect, structural parameters, and internal rotation in the molecule glycidaldehyde, (which

is a carbonyl derivative of ethylene oxide), and to compare these findings with those from a series of related compounds, cyclopropylcarboxaldehyde (10), cyclopropanecarboxylic acid fluoride (11), cyclopropyl methyl ketone(12), and vinylcyclopropane (13), previously studied in this laboratory. Theoretical and experimental aspects of microwave spectroscopy are given in Chapters II and III, and the results of the study on glycidaldehyde are given in Chapter IV.

Part Two of the thesis is concerned with the determination of the rates of rotational relaxation in carbonyl sulfide and ammonia, and begins with Chapter V.

2.1

som

sim

the

vib

mos

fro

mol

are

does

that

whic

give

Hers

make

ciabl

of th

inert

from

II. THEORY

2.1 Introduction

When one is attempting to determine expressions for the energy of some molecular system it is obviously most convenient to work with as simple a physical model as possible which still adequately describes the system. Wilson and Howard (14) have shown that rotational and vibrational energy are approximately separable and consequently for most purposes the rotational analysis can be carried out independently from any vibrational analysis. For treatment of the rotational motion, molecules may be viewed as collections of atoms with point masses which are fixed in some rigid configuration. This rigid rotor approximation does not ignore the vibrations within the molecule, but simply assumes that these vibrations yield some effective values for the bond distances, which can then be treated as though they were constant.

Though this traditional model of point masses and rigid bonds gives a very good fit to the rotational spectra of most molecules, Herschbach and Laurie (15) have pointed out that molecular vibrations make the "effective" moments of inertia obtained from this model appreciably different from the moments for the actual equilibrium structure of the molecule. However, they have also found that the moments of inertia for the average configuration of a molecule may be determined from the observed "effective" moments by applying corrections dependent

on t

poss

mon

2.2

res

For

by

The

the

mon

Whe

axi

mon

are

Exp

on the harmonic part of the vibrational potential. As a result, it is possible to determine average molecular structures from "effective" moments of inertia.

2.2 Moments of Inertia (16)

The moments of inertia depend on the positions of the masses with respect to the center of mass (COM) and the Cartesian coordinate system. For a molecule composed of N atoms the location of the COM is defined by the expression

$$\sum_{i}^{N} m_i \vec{R}_i = 0. \qquad (2\text{-}1)$$

The m_i's are the masses of the atoms and the $\vec{R}_i$'s are the vectors from the COM to the atoms. For a system rotating about some axis, α, the moment of inertia about the axis α is given by

$$I_\alpha = \sum_i m_i r_i^{(\alpha)^2}, \qquad (2\text{-}2)$$

where $r_i^{(\alpha)}$ is the perpendicular distance of the mass, m_i, from the axis α. If the rigid rotor approximation is used, the rotational motion can be described in terms of a tensor whose diagonal elements are the moments of inertia,

$$I_{xx} = \sum_i m_i (y_i^2 + z_i^2). \qquad (2\text{-}3)$$

Expressions for I_{yy} and I_{zz} are obtained by permuting x, y, and z.

The

iner

prod

pal

the

be d

orth

cosi

addi

tra-

whe

2.3

rot

whe

The off-diagonal elements of the inertia tensor are the products of inertia,

$$I_{xy} = -\sum_i m_i x_i y_i . \qquad (2\text{-}4)$$

If the proper orientation of the inertial axes is chosen, the products of inertia vanish and the moments of inertia are called principal moments. The principal moments of inertia are the eigenvalues of the inertia tensor. The inertia tensor is symmetric and may therefore be diagonalized by an orthogonal transformation. The elements of the orthogonal matrix which diagonalizes the inertia tensor are the direction cosines of the principal axes with respect to the original axes. In addition, the trace of the inertia tensor is invariant to an orthogonal transformation, so that

$$I_{xx} + I_{yy} + I_{zz} = I_a + I_b + I_c , \qquad (2\text{-}5)$$

where I_a, I_b, and I_c are the principal moments of inertia.

2.3 Rigid Rotor Hamiltonian

The rigid rotor Hamiltonian for a molecule written in terms of rotational constants A, B, and C is

$$H = \frac{4\pi^2}{h}(AP_a^2 + BP_b^2 + CP_c^2) , \qquad (2\text{-}6)$$

where $A = \frac{h}{8\pi^2 I_a}$, etc. and P_a, P_b, and P_c are the components of the total

angular momentum P along the principal axes a, b, and c, respectively. The rotational constants are conventionally chosen such that $A \geq B \geq C$ and are usually given in units of MHz.

The components of the angular momentum are related to the total angular momentum by the expression

$$P^2 = P_x^2 + P_y^2 + P_z^2. \tag{2-7}$$

It can be shown (17) that certain commutation relationships exist between the components of the angular momentum. In a molecule-fixed axis system they are as follows:

$$\begin{aligned} [P_x, P_y] &= -i\hbar P_z \,, \\ [P_y, P_z] &= -i\hbar P_x \,, \\ [P_z, P_x] &= -i\hbar P_y \,. \end{aligned} \tag{2-8}$$

As a result of these commutation relations, a closed form solution to the Schrödinger equation $H\Psi = E\Psi$ cannot be obtained if all three rotational constants are different and none is zero. If two rotational constants are equal, as is the case for a symmetric top molecule, a closed form solution can be obtained. When $A > B = C$ the molecule is referred to as a prolate symmetric top and when $A = B > C$ as an oblate symmetric top. A solution to the asymmetric rotor may be obtained by using the eigenfunctions of one of the two symmetric rotors as the basis functions for the solution.

In order to solve the rotational Schrödinger equation, it is convenient to obtain general expressions for the matrix elements of the total rotational angular momentum and for the individual components of angular momentum. It can be shown (18) by using equations (2-8) that the square of the total angular momentum commutes with any one of the components P_x, P_y, and P_z. It is possible then to simultaneously diagonalize the matrix of the square of the total angular momentum and that of any one component of P.

In a basis in which $P^2 = P_x^2 + P_y^2 + P_z^2$ and P_z are diagonal the only nonzero elements of the various angular momenta are found to be (19)

$$\langle J,K|P^2|J,K\rangle = J(J+1)\hbar^2 ,$$

$$\langle J,K|P_z|J,K\rangle = K\hbar ,$$

$$\langle J,K|P_x^2|J,K\rangle = \langle J,K|P_y^2|J,K\rangle = \frac{\hbar^2}{2}[J(J+1)-K^2] , \qquad (2\text{-}9)$$

and $$\langle J,K|P_x^2|J,K\pm2\rangle = -\langle J,K|P_y^2|J,K\pm2\rangle =$$

$$\frac{-\hbar^2}{4}[(J\mp K)(J\pm K+1)(J\mp K-1)(J\pm K+2)]^{1/2} .$$

Here J is the rotational quantum number which measures the total rotational angular momentum and K is the quantum number which measures the component of P along the z-axis.

In a symmetric rotor the Hamiltonian is diagonal in both the quantum numbers J and K and leads to the energy expression for a prolate top of the form

$$E = hBJ(J+1) + h(A-B)K^2. \qquad (2\text{-}10)$$

For this expression the axis representation I^r in which x ↔ b, y ↔ c, z ↔ a has been chosen (20). For an oblate top the energy is

$$E = hBJ(J+1) + h(C-B)K^2 \qquad (2\text{-}11)$$

if the axis representation III^ℓ (x ↔ b, y ↔ a, z ↔ c) is chosen.

In an asymmetric rotor J is still a good quantum number but K is not, because the projection of the total angular momentum is no longer constant along any axis fixed in the molecule. Even though K is no longer a good quantum number it is kept to help label the energy levels of the asymmetric rotor. Each level is then labeled with the notation J_{K_{-1},K_1}, where K_{-1} is the limiting value of K for the prolate top and K_1 is the limiting value for the oblate top.

In the symmetric rotor representation the energy matrix for an asymmetric rotor has elements which are off-diagonal in K. It is necessary to diagonalize this matrix to obtain the energy values for the asymmetric rotor. The matrix is symmetric and has off-diagonal elements removed by only two above and below the diagonal. By applying the Wang transformation (21) each submatrix corresponding to a given J can be factored into four smaller submatrices, two for K even and two for K odd. The eigenvalues of these submatrices are the values of the rotational energy. The Wang transformation causes a basis composed of functions of the form $\Psi(J,K)$ to be transformed to a basis of functions like $[\Psi(J,K) \pm \Psi(J,-K)]$.

The classification of transitions between energy levels of the asymmetric rotor is done in a number of ways (22). It may be shown that for dipole-allowed transitions ΔJ can be 0 or ±1, and ΔK_{-1} and

ΔK_1 can be 0, ±1, ±2, ... For $\Delta J = 0, -1$, and +1, the transitions are designated as Q, P and R branch, respectively. The molecular dipole moment $\vec{\mu}$ of an asymmetric top is not restricted to lie along a figure axis and therefore may have components in any or all principal axis directions. For a nonzero component of $\vec{\mu}$ along the a-axis ($\vec{\mu}_a$) the selection rules are ΔK_{-1} is even and ΔK_1 is odd and the intensity of a-type transitions is proportional to μ_a^2. Likewise, for $\mu_b \neq 0$, ΔK_{-1} is odd and ΔK_1 is odd, and the intensity is proportional to μ_b^2; and for $\mu_c \neq 0$, ΔK_{-1} is odd and ΔK_1 is even, and the intensity is proportional to μ_c^2. The transitions are generally referred to as a-type, b-type, and c-type, respectively, and the most intense transitions are those where ΔK_{-1} and ΔK_1 change by zero or one.

2.4 Stark Effect (23, 24)

When a molecule with an electric dipole moment, $\vec{\mu}$, is exposed to a static electric field, $\vec{\varepsilon}$, the component of the total angular momentum in the direction of the field is restricted to 2J+1 possible values. These values are associated with the quantum numbers M = 0, ±1, . . . , ±J which measure (in units of $\hbar$) the projection of J in the direction of the static field. This interaction, called the Stark effect, is treated by adding a term to the Hamiltonian for the rotor. The term added is

$$H_\varepsilon = -\vec{\mu} \cdot \vec{\varepsilon} = -\mu\varepsilon\cos\theta, \qquad (2\text{-}12)$$

where θ is the angle between the dipole moment and the field. From Eq. (2-12) it can be seen that the Stark effect is a function of the

dipole moment and the static electric field and may provide a method for determining the magnitude of the dipole moment for any molecule.

The Hamiltonian including the Stark effect is ordinarily partially diagonalized by means of perturbation theory. First-order and second-order Stark effects can occur. In order for a first-order Stark effect to be present, a molecule must have an average nonzero component of the dipole moment lying along the rotational angular momentum vector $\vec{J}$ in the absence of any external field. This can only be satisfied by the presence of an energy level degeneracy such as the K degeneracy in symmetric tops. The first-order energy correction to the Hamiltonian is given as

$$E_j^{(1)} = \langle \psi_j^{(0)} | H_\varepsilon | \psi_j^{(0)} \rangle \tag{2-13}$$

and the first-order Stark energy in the symmetric rotor basis is

$$E^{(1)} = \frac{-\mu \varepsilon K M}{J(J+1)}. \tag{2-14}$$

If no average nonzero component is present within the molecule, the first-order Stark effect will vanish, but the field may induce a component of $\vec{\mu}$ along $\vec{J}$ which can then interact with the field to cause a second-order Stark effect. It is the second-order Stark effect that is important in asymmetric rotors. The energy correction to the Hamiltonian for second-order Stark effects is given by

$$E_i^{(2)} = \sum_{j \neq i} \frac{|\langle \psi_i^{(0)} | H_\varepsilon | \psi_j^{(0)} \rangle \langle \psi_j^{(0)} | H_\varepsilon | \psi_i^{(0)} \rangle|}{E_i^{(0)} - E_j^{(0)}}, \tag{2-15}$$

with the final second-order energy expression being

$$E^{(2)}_{J_{K-1},K_1} = \sum_g (A_{gJ_{K-1},K_1} + M^2 B_{gJ_{K-1},K_1}) \mu_g^2 \epsilon^2, \qquad (2\text{-}16)$$

where g = a, b or c. Here A_{gJ} and B_{gJ} are constants which result from evaluation of Eq. (2-15) and which depend only on the molecular rotational constants. It can be seen from Eq. (2-16) that $E^{(2)}$ also depends on M^2.

The Michigan State University spectrometers are constructed so that the microwave radiation field and the static electric field, $\vec{\epsilon}$, are parallel. This results in the selection rule $\Delta M = 0$, and gives, for the shifts in the frequencies in the presence of the field, the expression

$$\nu_s = \sum_g (\Delta A_g + M^2 \Delta B_g) \mu_g^2 \epsilon^2. \qquad (2\text{-}17)$$

The ΔA_g and ΔB_g represent the differences in the A_{gJ} and B_{gJ} for the energy levels involved in the transition.

The Stark field splits the energy levels into J+1 components, where J is the lower energy level involved in the transition. The relative intensities of the Stark components for a transition are given by M^2 for Q branch transitions and $(J+1)^2 - M^2$ for P or R branch transitions. The assignment of a low J transition can often be made from its characteristic Stark pattern.

It can be seen from Eq. (2-17) that a plot of ν vs. ϵ^2 for one of the Stark components of a transition will yield a slope which is a linear combination of the dipole moment components, μ_g, for the

molec

trans

be so

The t

the e

molecule. Three such plots, when made with at least two different transitions, will lead to a set of three independent equations that can be solved to yield the three dipole moment components of the molecule. The total dipole moment of the molecule can then be obtained using the expression

$$\mu^2 = \sum_g \mu_g^2. \qquad (2\text{-}18)$$

III. EXPERIMENTAL

3.1 The Microwave Spectrometer

The microwave spectrum of glycidaldehyde was examined with two different Hughes-Wilson Stark modulated spectrometers (7) equipped with phase-sensitive detection.

Assignment of the microwave spectrum and the Stark effect studies were carried out in the P-band (12-18 GHz) and K-band (18-26.5 GHz) regions on a laboratory-assembled spectrometer equipped with 100 kHz modulation. The radiation sources were backward wave oscillators (BWOs) which were used because of their superior sweeping characteristics compared to the older reflex klystron. Sweeping of a BWO in the MSU system is accomplished by simply imposing the signal from a function generator (Wavetek Model 112S78) on the helix of the BWO. The sample cell consisted of a 12 ft. piece of X-band waveguide fitted with the usual Stark septum over its entire length. A cross-section of the Stark cell is shown in Figure 1. Detection of the modulated absorption signal was accomplished by rectification in a tunable silicon diode crystal detector followed by amplification and detection in a 100 kHz lock-in amplifier (PAR Model 120). The output of the lock-in detector was displayed on either a strip chart recorder or an oscilloscope. Frequency measurements were made by comparison of the absorption frequency with frequency markers which could be generated and measured to an accuracy

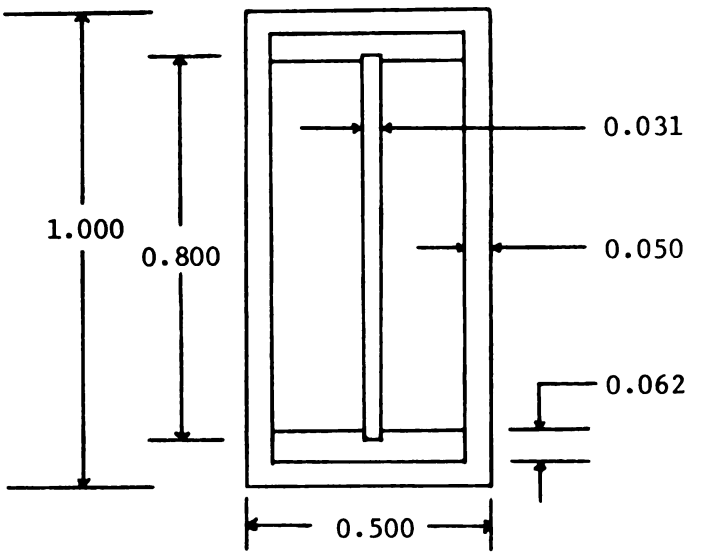

a - conventional design

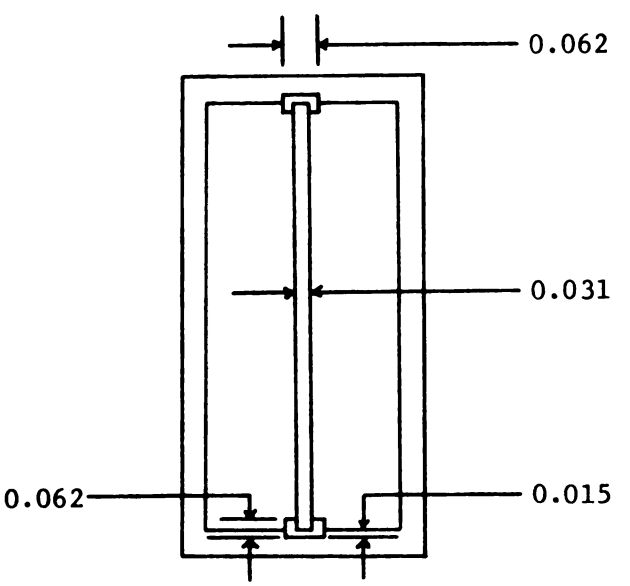

b - new design

Figure 1. Cross-Sections of Sample Cells (dimensions in inches).

of on

on a

spec

is g

oper

3.2

freq

cont

ove

and

turn

524

a s

wav

whi

sou

of

and

que

*

Mer

Mer

of one part in 10^7.

Intensity measurements were made in the R-band (26.5-40 GHz) region on a Hewlett-Packard Model 8460A molecular rotational resonance (MRR) spectrometer (25) which operates at a modulation frequency of 33 kHz.

A block diagram of a typical Stark-modulated microwave spectrometer is given in Figure 2. A more detailed discussion of the components and operation of a typical spectrometer may be found elsewhere (26-30).

3.2 Frequency Measurements

Frequency markers were generated by a Micro-Now Model 101c electronic frequency multiplier. This instrument employs a tunable 5 MHz crystal-controlled oscillator and is capable of generating markers every 50 MHz over the entire microwave region. The 5 MHz oscillator is monochromatic and stable to a few parts in 10^8. It was monitored for accuracy and tuned to ±1 Hz by means of a Hewlett-Packard frequency counter Model 5245L. The output of the marker generator is multiplied and mixed with a sample of the microwave radiation in a silicon diode mounted in the waveguide. The mixer is coupled to a Collins Model 51S-1 radio receiver which is used to determine the difference in frequency between the source radiation and a harmonic of the marker generator. The frequency of the radio receiver was varied until a super-position of a marker and the transition appeared on the dual beam oscilloscope. The frequency of the transition was then given by the frequency of the marker ± the receiver frequency. By using this technique frequency measurements were made to an accuracy of ±0.05 MHz. Rough frequency measurements were usually made first with a waveguide frequency meter so as

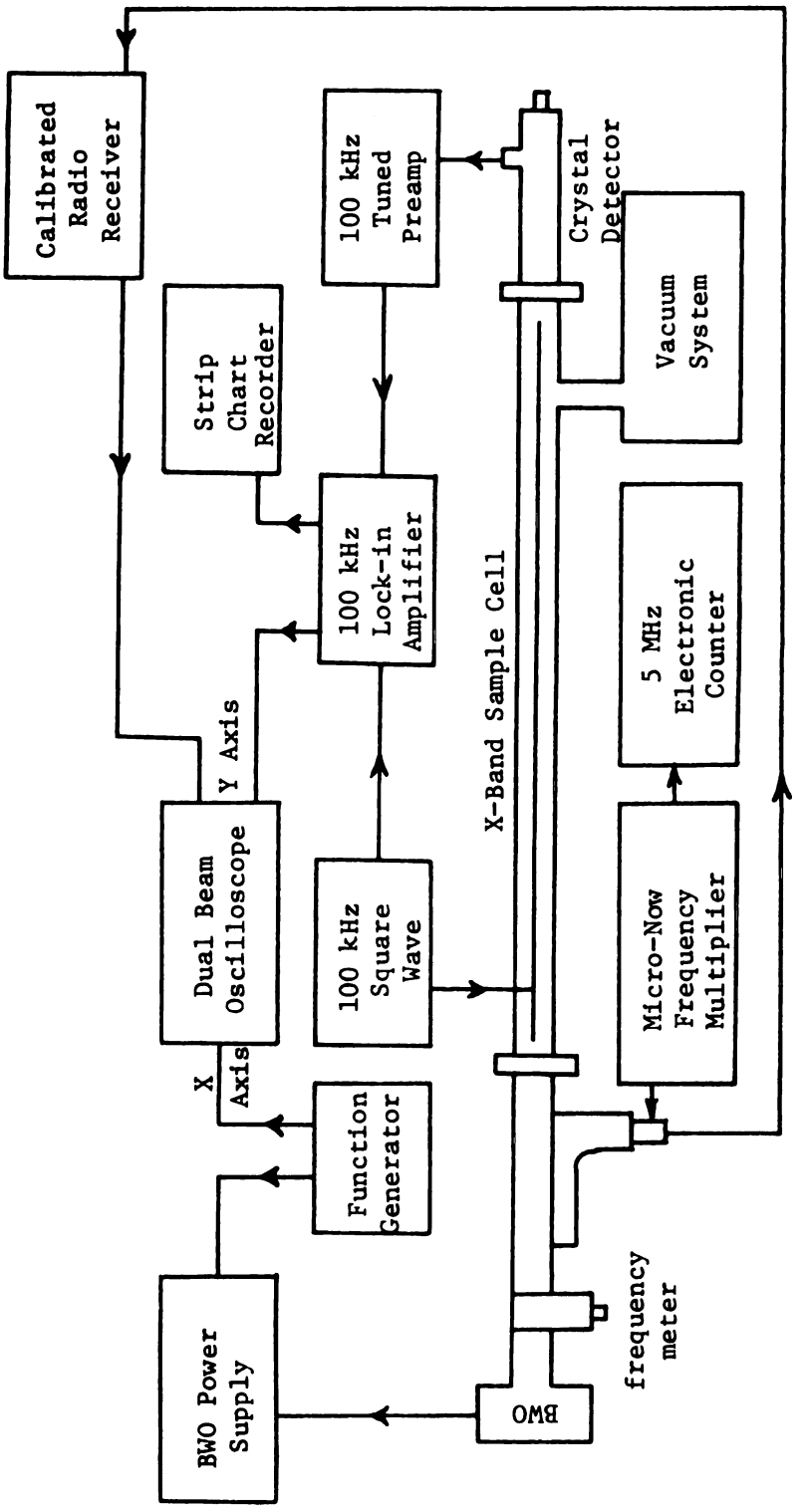

Figure 2. Block Diagram of a Typical MRR Spectrometer.

to quickly determine the frequency of the harmonic nearest the transition to be measured.

It should be pointed out that this method becomes more difficult at higher frequencies because the harmonics of the marker generator become weaker at higher harmonic numbers.

3.3 Stark Effect

The Stark effect for each of the transitions was determined by following the displacement of the Stark components of the transition as a function of a DC voltage applied to the base of the modulating Stark voltage. The DC voltage was obtained from a precision high voltage supply (Fluke Model 412B) and was monitored for accuracy with a Heathkit EU-805 digital voltmeter. The effective DC electric field in the Stark cell was evaluated by standardizing the cell spacing with the $J = 0 \rightarrow 1$ transition of OCS ($\mu_{OCS} = 0.7152$ Debye (31)).

3.4 Intensity Measurements

Relative intensity measurements of corresponding transitions in the ground and lowest three excited vibrational states were all carried out on the Hewlett-Packard MRR spectrometer referred to earlier. These relative intensity measurements were used to approximate the energy level separations in the ground and lowest three excited states of trans-glycidaldehyde. A knowledge of the energy level separations in trans-glycidaldehyde allows an estimation to be made of the minimum potential barrier to any other species which may be present. The procedure used to obtain these energy level separations is described below.

The first step in making relative intensity measurements is to determine the pressure and temperature at which reasonably strong yet sharp transitions are observed. In the case of glycidaldehyde it was convenient to work at room temperature with a sample pressure of 15 mtorr. It is also important to be sure that no other transition of any significant intensity lies near enough in frequency to overlap the transition to be measured, as this would increase the effective signal. Likewise, the Stark voltage must be adjusted to insure that no Stark components overlap the transition since overlapping Stark components would decrease the signal.

After the above requirements are met, the frequency of the incident radiation is adjusted to the resonance frequency of the line to be measured and the microwave power is adjusted to give a convenient crystal current at which all the subsequent measurements will be made. The phase-sensitive detector and the strip chart recorder are then adjusted to give as nearly full scale deflection of the signal as possible.

The relative intensities of any two transitions are simply related to their phase-sensitive detector and recorder settings.

The relative intensities are directly proportional to the relative populations of any two states provided the linewidths are the same. It is easy then to apply Boltzmann's equation,

$$N_1/N_0 = \exp(-\Delta E/kT), \qquad (3\text{-}1)$$

to determine the relative energy separation ΔE between states.

IV. MICROWAVE SPECTRUM OF GLYCIDALDEHYDE

4.1 Introduction

In recent years a number of studies of the microwave spectra of molecules obtained as derivatives of cyclopropane have been carried out at Michigan State University. Among these studies is the work reported by Volltrauer and Schwendeman (10,11) on the molecules cyclopropylcarboxaldehyde and cyclopropanecarboxylic acid fluoride, a study by Lee (12) on methyl cyclopropylketone, and the most recent work done on vinylcyclopropane by Codding (13). The primary objective in each case has been to observe the conformations of the molecules and to determine the potential barriers between the conformers. The primary objective was realized completely only in the first study where both cis and trans species were found for the molecules under investigation. Lee found that the only species present in a sufficient amount to assign a spectrum was the species with the carbonyl group cis to the ring and Codding was able to assign only the species with the vinyl group trans to the ring. It was, therefore, not possible to do a complete analysis in these cases. The study of glycidaldehyde was undertaken because of its structural similarities to the molecules previously studied in these laboratories.

A preliminary study of glycidaldehyde was carried out by Assink and Schwendeman (32). This study was checked, corrected, and extended

by the author and the final results are reported here. Although again only one species--that with the carbonyl group trans to the ring--has been assigned, it has been possible to measure the frequencies of transitions in the ground and first three torsionally excited states of this species. Rotational constants have been obtained for these states and the dipole moment has been determined from measurements of the Stark effect on a number of ground state transitions.

The sample of glycidaldehyde was obtained from Aldrich Chemical Company, Milwaukee, Wisconsin, and used without further purification.

4.2 Rotational Constants

The preliminary values of the structural parameters for glycidaldehyde needed for the initial estimation of the rotational constants were obtained from the structure of ethylene oxide (33) and the bond lengths in ethanal (34). A list of the assumed parameters is given in Table I. The calculation of the rotational constants was done with the aid of the computer program STRUCT written by Dr. R. H. Schwendeman. The program STRUCT also provides a listing of the coordinates for each of the atoms in the principal axis system. The calculated values of the rotational constants and the atomic coordinates for trans-glycidaldehyde can be found in Table II. It can be seen from these calculated rotational constants that trans-glycidaldehyde is expected to be a near prolate symmetric top (i.e. $A > B \simeq C$). The orientation of trans-glycidaldehyde in the principal axis system is shown in the planar projections given in Figure 3. By using these planar projections and the dipole moments of ethylene oxide (1.88 D) and ethanal (2.48 D) (35) it should

Table I. Assumed Molecular Parameters for Trans-Glycidaldehyde.

r(CH)	= 1.083 Å[a]	<HCH, <HC_2C_3	= 116°[a]
r(CC)(ring)	= 1.470 Å[a]	<HC_1C_2, <$C_1C_2C_3$	= 117.4°[a]
r(C_2C_3)	= 1.500 Å[b]	<$C_2C_3O_9$	= 123°[b]
r(CO)(ring)	= 1.435 Å[a]	<$H_8C_3O_9$	= 127°[c]
r(C_3O_9)	= 1.210 Å[c]		

[a] Parameters taken from ethylene oxide.

[b] Parameters taken from ethanal.

[c] Estimated.

Table II. Coordinates[a] and Rotational Constants for Trans-Glycidaldehyde in the Principal Axis System Using the Assumed Parameters of Table I.

Atom	a	b	c
C_1	-1.429430	.724213	.045608
C_2	-.264906	-.026671	-.445268
C_3	.990226	.031073	.374065
H_4	-.129181	-.092069	-1.517738
H_5	-1.313919	1.275743	.970465
H_6	-2.084400	1.168654	-.693564
O_7	-1.393602	-.708130	.121198
H_8	.742935	.094598	1.426539
O_9	2.097305	.007316	-.113696
	A = 18,243.9 MHz		
	B = 3,248.5 MHz		
	C = 3,107.9 MHz		

[a] in Å.

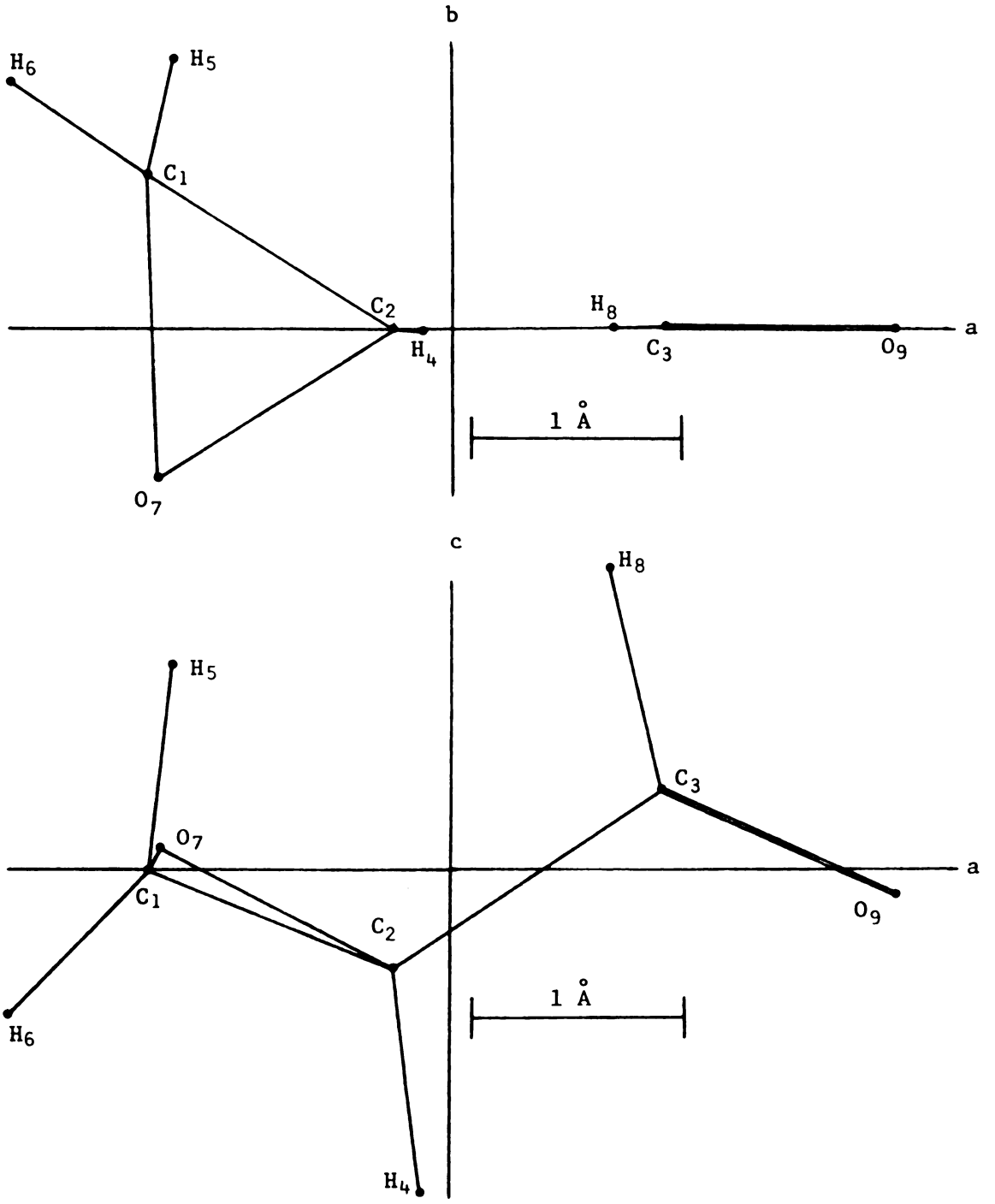

Figure 3. Planar Projections of Trans-Glycidaldehyde.

be possible to predict approximate values for the dipole moment components of trans-glycidaldehyde. Results of this prediction indicated that the a and b components of the dipole moment are essentially equal (1.65 D) and that the c component is zero or very close to zero. From these results one would anticipate that the strong transitions in the microwave spectrum are a-type and b-type transitions.

The calculated rotational constants and the probable values of the dipole moment components were then used in the computer program EIGVALS written by Schwendeman and Hand (36) to calculate an approximate spectrum. This spectrum was then used as a guide during the initial search for an assignment.

The spectrum of glycidaldehyde was rich in strong lines with characteristic Stark effects and afforded easy identification of a number of transitions. These transitions were attributed to a b-type Q-branch series found in the P-band region (12.4-18.0 GHz) and to an a-type R-branch series found in the K-band region (18.0-26.5 GHz). As expected, it was not possible to find any strong c-type transitions; however, a number of low J Q-branch lines were assigned (32). The Stark effect was carefully observed for several transitions and a search for excited states was made. As many as four excited states were observed for a number of transitions and frequency measurements were made wherever possible. From the frequencies of both a-type and b-type transitions for the ground and excited states accurate values for all three rotational constants were obtained. The observed transition frequencies for trans-glycidaldehyde are given in Table III and the derived rotational constants, moments of inertia, and second moments can be found in Table IV. The regular progression of rotational constants indicates

Table III. Frequencies[a] of Transitions for Trans-Glycidaldehyde in the Ground and First Three Excited States.

Transition	v=0	v=1	v=2	v=3
0_{00}-1_{11}	21,378.78(0.10)[b]			
1_{11}-2_{12}	12,686.03(0.07)			
1_{01}-2_{02}	12,820.36(0.14)			
2_{02}-2_{12}	14,833.74(-0.11)			
2_{02}-2_{11}	15,239.45(0.07)	15,103.35(0.06)	14,970.93(0.09)	
2_{12}-3_{13}	19,028.44(-0.33)	19,070.91(-0.04)	19,112.97(-0.24)	19,149.48(0.14)
2_{02}-3_{03}	19,228.22(0.17)			
2_{21}-3_{22}	19,231.62(-0.08)			
2_{20}-3_{21}	19,235.20(-0.14)			
2_{11}-3_{12}	19,434.01(0.12)	19,499.73(0.08)	19,564.70(-0.15)	19,622.24(-0.01)
3_{03}-3_{13}	14,633.93(-0.24)			
3_{03}-3_{12}	15,455.23(0.01)	15,321.11(-0.00)	15,200.53(-0.02)	
3_{13}-4_{14}	25,370.08(-0.02)	25,426.65(-0.10)	25,482.56(-0.38)	25,531.14(-0.11)
3_{03}-4_{04}	25,633.34(0.18)	25,704.38(0.07)	25,775.47(0.67)	25,838.18(0.02)

continued

Table III (cont'd.)

Transition	v=0	v=1	v=2	v=3
4_{04}-4_{14}	14,370.73(-0.39)			
4_{04}-4_{13}	15,722.84(-0.01)	15,615.10(-0.03)	15,510.87(0.02)	
5_{05}-5_{15}	14,046.91(-0.54)			
5_{05}-5_{14}	16,074.95(-0.02)	15,988.38(-0.01)	15,905.16(-0.01)	
6_{06}-6_{15}	16,504.90(-0.06)	16,444.67(-0.02)	16,387.65(-0.07)	
7_{07}-7_{16}	17,016.68(-0.09)			

[a] In MHz. Uncertainty in observed frequencies is ±0.05 MHz.

[b] Values in parentheses are observed minus calculated frequencies; rotational constants are in Table IV.

Table IV. Rotational Constants[a], Moments of Inertia[b], and Second Moments[b] for Trans-Glycidaldehyde.

	v=0	v=1	v=2	v=3
A	18,240.99	18,102.23	17,967.14	
B	3,272.87	3,285.78	3,298.57	3,309.89
C	3,137.70	3,142.87	3,148.02	3,152.26
I_a	27.7055	27.9179	28.1278	
I_b	154.4137	153.8072	153.2108	152.6865
I_c	161.0660	160.8007	160.5380	160.3220
P_{aa}	143.8871	143.3450	142.8105	
P_{bb}	17.1789	17.4556	17.7275	
P_{cc}	10.5266	10.4622	10.4003	

[a] In MHz. Uncertainties in rotational constants are ±0.05 MHz.

[b] In u.$\mathring{A}^2$.

that the excited states are excitations of the same mode.

A preliminary study of the recordings of the spectrum of glycidaldehyde indicated that the intensities of the transitions decreased by about a factor of two between successive excited states. This corresponds to a rather low vibrational energy separation between states and is most likely due to a torsional motion of the aldehyde group about the carbon-carbon bond.

The rotational constants of glycidaldehyde are plotted as a function of the torsional angle θ in Figure 4. The A rotational constant has a strong dependence on θ and near the trans configuration ($\theta = 0°$) A is equal to the experimental value. By contrast, B and C have a rather weak dependence on θ near the trans configuration. The B and C rotational constants each correspond to two possible values for θ which are symmetrically placed about $\theta = 0°$. From Figure 4 it can be seen that the three rotational constants do not predict quite the same value for θ. This suggests that there is an error in one or more of the structural parameters used in the original calculation of the rotational constants. A simple analysis of the angular dependence of the aldehyde group to the ring was carried out which showed that the rotational constants could be fit by this adjustment alone. Only minor changes in the angular structural parameters of the aldehyde group were required to achieve a fit and hence the originally proposed structure of trans-glycidaldehyde was left as correct. To do a complete structural analysis would require extensive isotopic substitution, a task beyond the scope of this study.

A plot of the changes in the rotational constants as a function of the quantum number of the excited states is given in Figure 5. The

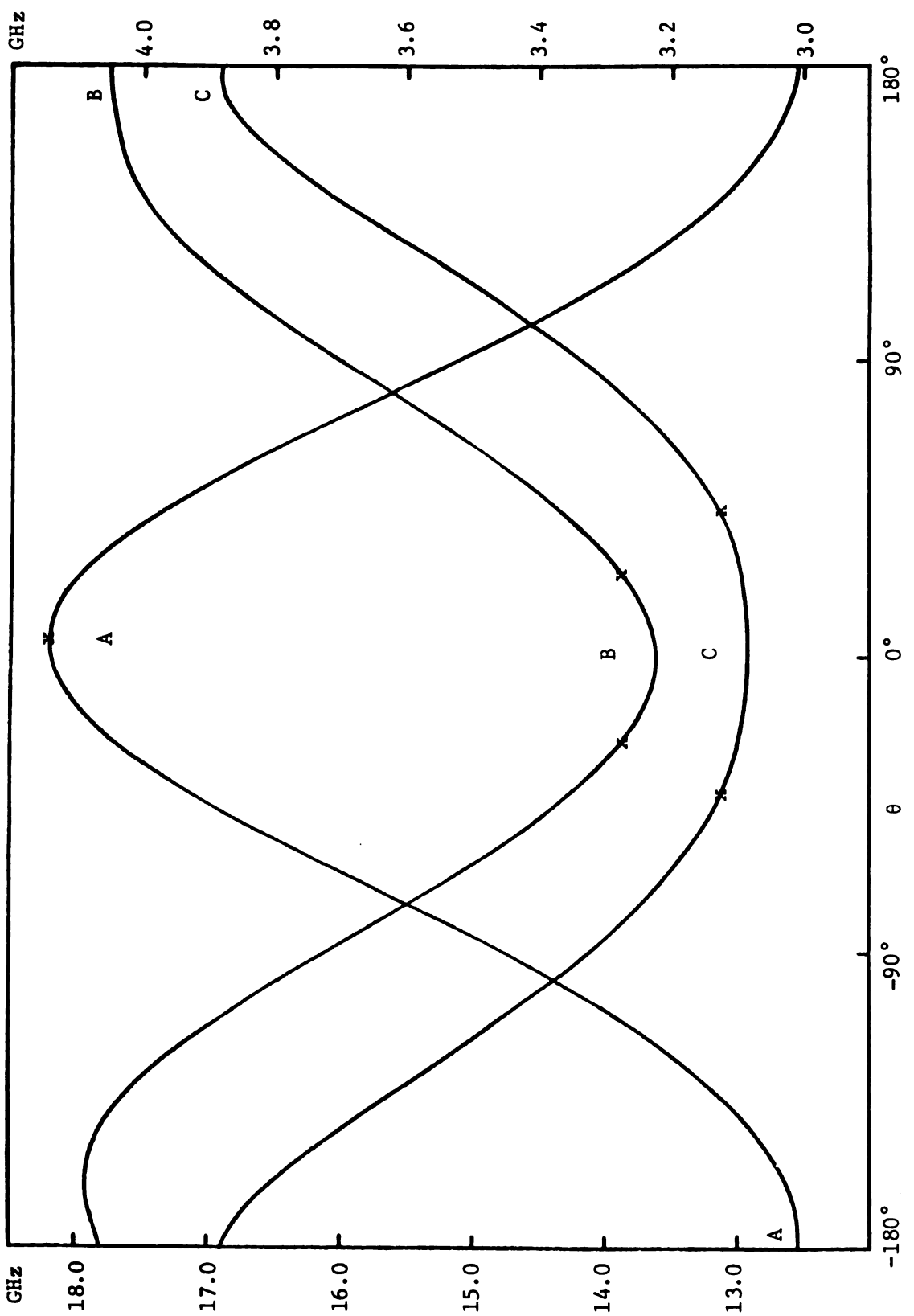

Figure 4. The Rotational Constants of Glycidaldehyde Plotted[a] as a Function of the Torsional Angle θ of the Aldehyde Group.

Trans-glycidaldehyde is for θ = 0°.

[a] Scale at left is for A; scale at right is for B and C.

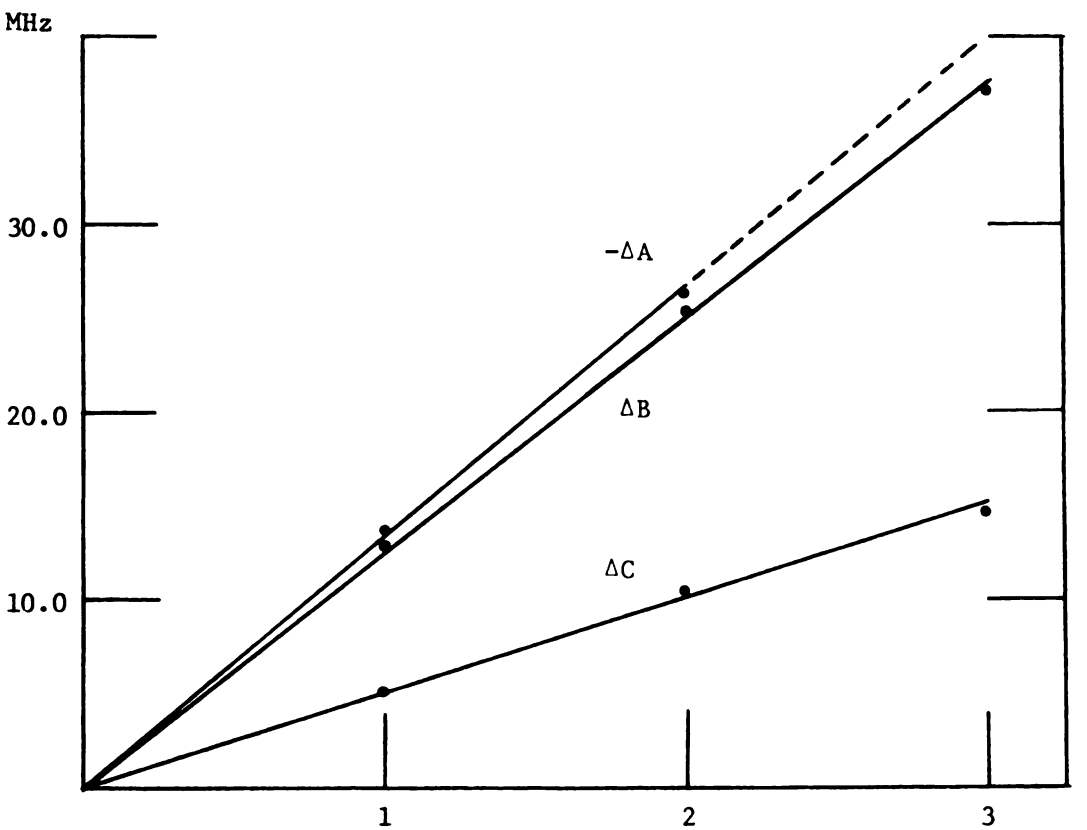

Figure 5. Change of Rotational Constants (in MHz) as a Function of the Vibrational State.

-ΔA has been reduced by a factor of 10.

Dashed portion of -ΔA is a projection to the third vibrational state.

plot is very nearly linear which implies that the vibrational motion is essentially harmonic. A comparison of the variation of the rotational constants of the excited states to the variation with the angle of rotation θ about the carbon-carbon bond for θ near 0° leaves little doubt that the excited states are the result of the torsional motion.

An extensive search for other transitions which could be attributed to the presence of other species proved unsuccessful. The cis species and one gauche species were predicted to have large dipole moments; the second gauche form was predicted to have a rather small dipole moment. The failure to observe transitions in a second species suggests that the cis-trans (or gauche-trans) energy separation is at least one kcal/mole. The potential barrier separating the cis and trans or cis and gauche species must be at least this large and may be even larger.

4.3 Dipole Moment

The molecular dipole moment of trans-glycidaldehyde was determined from a plot of ν vs. ε^2 (as suggested by Eq. (2-17)) for the M=1 Stark component of the 2_{12}-3_{13} transition and two Stark components from each of a pair of Q-branch transitions, the 4_{04}-4_{13} and the 5_{05}-5_{14}. A least squares analysis of the slopes $\frac{\partial \nu}{\partial \varepsilon^2}$ from these plots was used to determine the three components of the dipole moment. As predicted in Section 4.2, μ_a and μ_b are of the same order of magnitude with μ_a slightly larger. This was also reflected in that the b-type transitions of comparable linestrength are less intense than the a-type. The value of μ_c was greater than zero by more than the expected error and therefore was assumed to be nonzero though small. The experimental

values obtained for μ_a, μ_b, μ_c and μ_T are given in Table V along with a comparison of the calculated and experimental Stark shift slopes. A comparison of dipole moments for trans-glycidaldehyde and a number of various related compounds is given in Table VI.

The ratio $(\mu_i/\mu_j)^2$ reflects the relative intensities of any pair of transitions dependent on the dipole components μ_i and μ_j. Using the ratio $(\mu_c/\mu_a)^2$ to predict the intensities of the c-type transitions relative to the a-type clearly points out why the c-type transitions were so weak and difficult to locate.

4.4 Relative Intensity Measurements

Excited state relative intensity measurements were made on the 4_{13}-5_{14} and 4_{14}-5_{15} R-branch transitions located in the R-band region (26.5-40 GHz). Measurements were made through the third excited state and showed that the relative intensities of any pair of successive states were equal. The intensity ratio was 0.51 and corresponds to an energy separation between states of 140 cm^{-1}. This common intensity ratio for successive states indicates that the potential function separating these states is essentially harmonic; the same conclusion was obtained in Section 4.2 by analysis of the rotational constants.

4.5 Discussion

The results of this study indicate that the major conformation present in gaseous glycidaldehyde is the trans species. This configuration of the aldehyde group puts the oxygen atom in close proximity to the ring hydrogen allowing a possible increased interaction of a

Table V. Stark Effect and Dipole Moment of Trans-Glycidaldehyde.

Transition	(M)	$d\nu/dE^2$(obs.)[a,b]	$d\nu/dE^2$(calc.)[a]
2_{12}-3_{13}	1	62.33	62.33
4_{04}-4_{13}	3	28.91	28.84
4_{04}-4_{13}	4	55.46	55.41
5_{05}-5_{14}	4	24.18	24.18
5_{05}-5_{14}	5	40.08	40.20

μ_a = 1.932 ± 0.005 D

μ_b = 1.511 ± 0.017 D

μ_c = 0.277 ± 0.156 D

μ_T = 2.469 ± 0.031 D

[a] Hz/(volt/cm)^2 assuming μ_{ocs} = 0.7152 D.

[b] Uncertainty in observed slopes is ± 0.5%.

Table VI. Dipole Moment of Trans-Glycidaldehyde and Some Related Compounds.

Compound		U_T[a]	Ref.
Acetaldehyde (Ethanal)		2.48	(35)
Ethylene Oxide		1.88	(35)
Cyclopropylcarboxaldehyde	(cis)	2.74	(10)
	(trans)	3.26	
Cyclopropanecarboxylic Acid Fluoride	(cis)	3.28	(11)
	(trans)	3.47	
Cyclopropyl Methyl Ketone	(cis)	2.62	(12)
Glycidaldehyde	(trans)	2.47	(This work)

[a] The total dipole moment in Debyes.

stabilizing nature. The trans configuration also decreases any hydrogen-hydrogen interaction that would be present if a cis conformation were present. It is not surprising then that the trans species is the dominant one. The presence of a cis or gauche species was anticipated but could not be found though a thorough investigation was made. Based on dipole moment estimates the cis species should have had as large a dipole moment as the trans species. Since no transitions could be assigned to a second species, one of two possibilities is indicated: either the cis species is present in too small an amount to be observed, or some vibration-rotation interaction is radically altering its spectrum.

The lack of any assignable species except the trans species defeated the primary objective of this work which was the calculation of the barrier to internal rotation. Consequently a comparison to the work done by Volltrauer and Schwendeman cannot be made. The observation of four excited states each separated by an energy of 140 cm^{-1} would imply, however, that any barrier present between the trans and any other species would be at least 2 kcal/mole.

The dipole moment of trans-glycidaldehyde obtained was that expected based on dipole moments observed in similar molecules (Table VI). The lack of a plane of symmetry resulted in all three components of μ_T being nonzero, though μ_c was very nearly zero due to a near cancellation of the μ_c component of the ring by that from the aldehyde group. This same cancellation took place along the a-axis, but to a lesser degree, and could explain why the dipole moment of trans-glycidaldehyde is about 1 Debye less than the trans species of the related compounds.

PART 2: ROTATIONAL RELAXATION IN CARBONYL SULFIDE AND AMMONIA

V. INTRODUCTION

The investigation of collision-broadened line shapes has long been a method of determining rotational relaxation in gases. One of the earlier works was the semiclassical treatment of line shapes and mechanisms for line broadening made by Van Vleck and Weisskopf (37). Later Anderson (38) introduced another semiclassical treatment which investigated line broadening due to molecular collisions. In each of these investigations the radiation incident upon the gas was a low-power radiation. Under these conditions, transitions among the molecular states are induced at a rate which is negligible compared with the collision rate and thermal equilibrium is maintained. The energy levels under investigation remain then in a Boltzmann distribution.

Karplus and Schwinger (39) and Snyder and Richards (40) extended the theories of line shape to include the case where partial saturation due to a high-power incident radiation is present. Saturation invalidates the assumption of thermal equilibrium and requires a quantum mechanical treatment of the effect of the radiation. Using a density matrix approach Karplus and Schwinger and Snyder and Richards independently calculated the same expression for the absorption coefficient for the steady state, i.e., a long time after the incident radiation was turned on. It was shown that the absorption line should have an additional broadening due to the radiation, and that this broadening is the result of the high power levels of the incident radiation which cause transitions among the

molecular states to occur at a rate that is not negligible compared with the collision rate.

Schwendeman (41) has recently used the density matrix approach to obtain the expression for the time dependent absorption coefficient for the case of partial saturation in the intermediate time scale, i.e., at times shortly after the incident radiation is turned on. It was found that the absorption coefficient varies with time as an exponentially damped oscillation. This expression, which contains the rate constant for rotational relaxation, was derived to explain the time-resolved spectra, or "wiggle-beat" spectra, which were first obtained by Harrington (42) and repeated and extended in these laboratories.

In an attempt to explain further certain phenomena observed in these laboratories, Pickett (43) has recently extended the theory of the intermediate time scale to include the effect of Stark modulation. It was found that this effect is important only when the incident radiation is tuned slightly off-resonance.

It is the purpose of Part Two of this thesis to characterize these "wiggle-beat" spectra for the molecules carbonyl sulfide and ammonia and to relate these wave shapes to recent theories. The molecules carbonyl sulfide and ammonia were chosen because of their strong and uncomplicated spectra. The initial studies of rotational relaxation behavior in gases conducted in these laboratories was done by Brittain (44) on the $J = 0 \rightarrow 1$ transition of OCS. The data from those studies also have been treated by this author and the results are presented here.

The development of the theories pertinent to the studies carried out in these laboratories is made in Chapter VI. A complete description

of the experimental method can be found in Chapter VII, and a discussion of the "wiggle-beat" line shapes with a comparison to the theory is given in Chapter VIII.

VI. THEORY

6.1 Density Matrices (45)

For the purpose of this study the gas under investigation will be considered as an ensemble of identical non-interacting molecules or quantum mechanical systems. The state of each system can be represented by a set of time-dependent numbers, a(n,t), which are the coefficients for expanding the probability amplitude in coordinate language. This expansion has the following form:

$$\Psi_\alpha(q,t) = \sum_k a_\alpha(k,t)U(k,q). \tag{6-1}$$

Here $\Psi_\alpha(q,t)$ is the wave equation defining the αth molecule, and the U(k,q) are any complete set of orthonormal eigenfunctions in the coordinate representation q.

The density matrix for an ensemble of N molecules or systems is then defined by its elements which are expressed as follows:

$$\rho_{nm} = \left(\frac{1}{N}\right) \sum_{\alpha=1}^{N} a_\alpha^*(m,t)a_\alpha(n,t) = \overline{a_m^* a_n}. \tag{6-2}$$

The sum α over all systems of the ensemble, as seen in the equation above, would imply the presence of a kind of ensemble average for the elements of the density matrix.

Since the U(k,q) are a complete set of orthonormal eigenfunctions, $W_n = a_n^* a_n$ gives the probability of finding an individual system α, described by $\Psi_\alpha(q,t)$, in the state corresponding to U(n,q). Similarly then, the expression $\rho_{nn} = \overline{\overline{a_n^* a_n}}$ gives the probability that a system α chosen at random from the ensemble would be found in state n. It also must follow then that $\sum_k \rho_{kk} = 1$, i.e., the trace of the density matrix must equal one, and that $N\rho_{nn}$ gives the population of state U_n.

For any observable F_α in a quantum mechanical system, the average value $\overline{F}_\alpha$ of that observable is given by the equation

$$\overline{F}_\alpha = \int \Psi_\alpha^* \hat{F} \Psi_\alpha \, dq. \tag{6-3}$$

Here $\hat{F}$ is the quantum mechanical operator associated with the observable F_α. Substitution for Ψ_α from Eq. (6-1) leads to the expression

$$\overline{F}_\alpha = \sum_{m,n} \int a_m^{(\alpha)*} U_m^{(\alpha)*} \hat{F} a_n^{(\alpha)} U_n^{(\alpha)} dq = \sum_{m,n} a_m^{(\alpha)*} a_n^{(\alpha)} F_{mn}^{(\alpha)} , \tag{6-4}$$

where $$F_{mn}^{(\alpha)} = \int U_m^{(\alpha)*} \hat{F} U_n^{(\alpha)} dq. \tag{6-5}$$

The calculation of the ensemble average $\overline{\overline{F}}$ for the observable is suggested by Eq. (6-2) and leads to the relation

$$\overline{\overline{F}} = \left(\frac{1}{N}\right) \sum_{\alpha=1}^{N} \overline{F}_\alpha. \tag{6-6}$$

Following the indicated prescription given by Eq. (6-6) results in an expression for the ensemble average of the observable F which is

dependent on the density matrix as follows:

$$\bar{\bar{F}} = \sum_{mn}\sum \rho_{nm}F_{mn} = \sum_{n}(\rho F)_{nn} = Tr(\rho F). \tag{6-7}$$

If we assume that the quantum mechanical operator $\hat{F}$ is time independent, then the time dependence of $\bar{\bar{F}}$ will depend on the time dependence of the density matrix.

The time dependence of the density matrix in terms of the total energy of the system can be determined by using the time dependent Schrödinger equation,

$$\hat{H}\Psi_{\alpha}(q,t) = i\hbar\frac{\partial\Psi_{\alpha}(q,t)}{\partial t}, \tag{6-8}$$

as the starting point. Substitution for Ψ_{α} from Eq. (6-1) yields the expression

$$\sum_{k} a_k^{(\alpha)*}\hat{H}U_k(q) = i\hbar\sum_{k}\dot{a}_k^{(\alpha)}U_k(q), \tag{6-9}$$

where superior dots signify derivatives with respect to time. Multiplication on the left side by U_n^* followed by integration results in the time derivatives of the $a_n^{(\alpha)}$. These are:

$$\dot{a}_n^{(\alpha)} = -\frac{i}{\hbar}\sum_{k}H_{nk}a_k^{(\alpha)} \text{ and } \dot{a}_n^{(\alpha)*} = \frac{i}{\hbar}\sum_{k}H_{nk}^{*}a_k^{(\alpha)*}. \tag{6-10}$$

Taking the definition of the density matrix from Eq. (6-2) and evaluating

it for its time derivative gives

$$\dot{\rho}_{nm} = \left(\frac{1}{N}\right) \sum_{\alpha=1}^{N} [\dot{a}_m^{(\alpha)*} a_n^{(\alpha)} + a_m^{(\alpha)*} \dot{a}_n^{(\alpha)}]. \tag{6-11}$$

Now substituting from Eq. (6-10) into Eq. (6-11) yields

$$\dot{\rho}_{nm} = \left(\frac{1}{N}\right) \left(\frac{-i}{\hbar}\right) \sum_{\alpha=1}^{N} \sum_{k} [H_{nk} a_m^{(\alpha)*} a_k - H_{mk}^{*} a_k^{(\alpha)*} a_n^{(\alpha)}] \tag{6-12}$$

which can be simplified, by using the fact that $H_{mk}^{*} = H_{km}$, to

$$\dot{\rho}_{nm} = \frac{-i}{\hbar} [(H\rho)_{nm} - (\rho H)_{nm}]. \tag{6-13}$$

Thus the standard form for the time dependence of the density matrix is given by

$$\dot{\rho} = \frac{-i}{\hbar} [H\rho - \rho H]. \tag{6-14}$$

In this equation H is the Hamiltonian for the system of interest.

6.2 The Absorption Coefficient (39-41)

The linear absorption coefficient α for incident electromagnetic radiation of angular frequency ω striking a gas of molecular density N is given by the expression

$$\alpha = 4\pi(\omega/c)N\mathrm{Im}(\chi), \tag{6-15}$$

where χ is the molecular susceptibility and c is the average group

velocity of the incident radiation. From Eq. (6-15) it can be seen that it is necessary to obtain an expression for χ in order to obtain α. The molecular susceptibility can be found from the dipole moment

$$\vec{p}(t) = \mathrm{Re}(\chi \vec{F}^{o} e^{-i\omega t}) \tag{6-16}$$

induced by the field

$$\vec{F}(t) = \mathrm{Re}(\vec{F}^{o} e^{-i\omega t}) = \vec{F}^{o} \cos\omega t. \tag{6-17}$$

Eq. (6-7) gives the prescription for finding the induced dipole moment, namely

$$\vec{p}(t) = \mathrm{Trace}[\rho(t)\vec{\mu}], \tag{6-18}$$

where $\vec{\mu}$ is the matrix operator for the permanent dipole moment of the molecule being irradiated. It can be seen from Eq. (6-18) that the time dependence of $\vec{p}(t)$, and consequently χ and α, will be determined by the time dependence of $\rho(t)$ as indicated in Eq. (6-14).

Eq. (6-14) indicates that it is necessary to express the Hamiltonian for the system under investigation. In the case of molecules being irradiated by high-power radiation the Hamiltonian should contain terms which reflect the state of the molecules themselves, the interaction between the molecules and the radiation, and the interaction of the molecules with each other through collisions. Because of the difficulty in treating the molecular collisions their effect is usually left out of the expression for the Hamiltonian and treated separately. The

Hamiltonian then becomes

$$H(t) = H^{o} - \vec{\mu} \cdot \vec{F}(t) = H^{o} + V\cos\omega t. \qquad (6\text{-}19)$$

In this equation H^{o} is the contribution to the Hamiltonian from the molecules themselves and is time independent; $V\cos\omega t$ is the contribution to the Hamiltonian due to the interaction of the molecules with the radiation and is time dependent. In this equation,

$$V = -\vec{\mu} \cdot \vec{F}^{o}. \qquad (6\text{-}20)$$

At this point there are two possible ways to proceed, either of which will give the time dependence of the absorption coefficient α. The first method is that of Karplus and Schwinger (39) in which they find a collision-averaged density matrix and then solve the resultant differential equation to obtain α. The second method is that of Snyder and Richards (40) in which they solve the density matrix differential Eq. (6-14) to obtain α and then collision-average this α. Schwendeman (41) has shown that both of these methods lead to the same α, and thus has shown that the point at which the collisions are treated is immaterial. The method used here will be the simpler method of Snyder and Richards.

In order to simplify the evaluation of the time dependent expression for the absorption coefficient α, it is advantageous to introduce several assumptions during the development of the theory. These are as follows: (a) $T_c << 1/\omega << \tau$, where T_c is the duration of the molecular collision, $1/\omega$ is the period of the incident radiation, and τ is the mean time

between molecular collisions; (b) only two energy levels are active in producing absorption; and (c) molecular collisions restore thermal equilibrium.

In order for assumption (a) to be valid the pressure must be kept low enough so that the collision diameter can be considered negligible compared with the mean free path length. Assumption (a) also suggests several different time scales. In the treatment here three time scales are considered. The first is the "short time" scale and refers to times of the order of $1/\omega$ or faster. Events that occur in this time scale are considered too fast to be observed by the experimental aparatus. The second is the "intermediate time" scale and is of the order of the mean time between collisions τ. The third is the "long time" scale and concerns times which are long compared to τ, i.e., at times long enough to establish a "steady-state" between the perturbation caused by the incident radiation and the mechanism for relaxation, which in this case is the molecular collisions. Thus, in the "steady-state" ρ, χ, and hence α approach constant values.

Assumption (b) implies that when the incident radiation of angular frequency ω is near the resonance frequency $\omega_o = (E_a^o - E_b^o)/\hbar$ for the active levels E_a^o and E_b^o, such that $(\omega - \omega_o) \simeq 1/\tau$ and all other resonance frequencies of the molecule are much larger than the difference $(\omega - \omega_o)$, it is necessary to consider only the terms in the subsequent derivation which oscillate with a frequency comparable to the difference $(\omega - \omega_o)$. Under these conditions the density matrix, and hence χ and α, oscillate with a frequency which is comparable to $1/\tau$. This is the "intermediate time" scale and the one of interest here.

Assumption (c) suggests that the molecular collisions are hard collisions, and that the effects of a collision are independent of the presence of the incident radiation. However, recently Oka (46-51) has shown that the concept of hard collisions is not completely correct. Nonetheless, in this case it leads to a perfectly reasonable result.

6.3 Collision Averaging (41)

Prior to the onset of the radiation the Hamiltonian which describes the ensemble will contain only the term H^o. The density matrix which describes the ensemble under these conditions is written as

$$\rho^o = C \exp(-H^o/kT), \tag{6-21}$$

where C is a normalization constant and is given by the expression

$$C = [Tr(\exp(-H^o/kT))]^{-1}. \tag{6-22}$$

In a basis set consisting of the eigenfunctions of H^o the only elements of the density matrix ρ^o which are nonzero are the diagonal elements. The distribution which describes the molecules under these conditions is the Boltzmann distribution. A set of boundary conditions, which is later used in the derivation of the expression for the absorption coefficient, is provided by the fact that all of the off-diagonal elements of the density matrix are zero at any time prior to the time when the radiation is turned on.

In the presence of the radiation field the Hamiltonian which describes the ensemble will not only contain H^o but now will also contain the term $V\cos\omega t$, which is due to the field. The density matrix which describes the ensemble under these conditions now contains nonzero off-diagonal elements whose magnitudes depend on the field strength V and the time. It will be assumed that after each collision the density matrix describing the ensemble will return to the density matrix ρ^o, given by Eq. (6-21). This provides an additional boundary condition which can be used in the derivation of the expression for the absorption coefficient.

In treating the effect of the collisions it will be assumed that the collisions occur at completely random time intervals. This assumption leads to an expression for the probability per molecule that at time t the last collision occurred in the time interval $t_o \rightarrow t_o + dt_o$. This expression is

$$\exp((t_o - t)/\tau)dt_o/\tau. \tag{6-23}$$

Integration of Eq. (6-23) over dt_o from time t = 0 (the time the radiation was first turned on) to time t gives an expression for the probability that a molecule has not undergone a collision between time t = 0 and the time of observation t. Integration of Eq. (6-23) yields

$$\int_o^t \exp((t_o-t)/\tau)dt_o/\tau = 1 - \exp(-t/\tau). \tag{6-24}$$

The sum of the probabilities for a molecular collision and for no molecular collision must be unity. Therefore, from Eqs. (6-23) and (6-24) it can be seen that the probability at time t that a given molecule has not collided since time t = 0 is

$$\exp(-t/\tau). \tag{6-25}$$

With expressions for the probability that a collision has or has not taken place since time t = 0, it is possible to write an expression for the collision averaged absorption coefficient at time t, as follows:

$$\bar{\alpha}(t) = \alpha(t,0)\exp(-t/\tau) + \int_0^t \alpha(t,t_o)\exp((t_o-t)/\tau)dt_o/\tau. \tag{6-26}$$

In Eq. (6-26), $\alpha(t,t_o)$ is the contribution to the absorption coefficient at time t from molecules which last collided at t_o, and the first term in Eq. (6-26) is the contribution from molecules which have not collided at all since time t = 0. The second term is the sum of the contributions to $\bar{\alpha}(t)$ from molecules which have collided since t = 0. The procedure suggested by this expression is the method used by Snyder and Richards mentioned earlier in Section 6.2. An explicit form of $\alpha(t,t_o)$ from the solution of the density matrix differential equation is all that is necessary to complete the solution for $\bar{\alpha}(t)$.

The alternate method used by Karplus and Schwinger starts with a collision-averaged density matrix of the form,

$$\bar{\rho}(t) = \rho(t,0)\exp(-t/\tau) + \int_0^t \rho(t,t_o)\exp((t_o-t)/\tau)dt_o/\tau\ , \tag{6-27}$$

which can be differentiated with respect to time to give the differential equation for $\dot{\bar{\rho}}(t)$ which must then be solved in order to obtain the time dependent absorption coefficient $\bar{\alpha}(t)$. The form of the differential equation for $\dot{\bar{\rho}}(t)$ is as follows:

$$\dot{\bar{\rho}}(t) = \frac{-i}{\hbar} (H\bar{\rho} - \bar{\rho}H) - \frac{1}{\tau} (\bar{\rho} - \rho_o). \tag{6-28}$$

Only the procedure of Snyder and Richards will be described here in detail. An expression for $\alpha(t,t_o)$ in the "intermediate time" scale, i.e., the time scale of interest here, has been derived by Schwendeman (41) and this derivation will be summarized in the following two sections.

6.4 Systems Without Collisions (41)

The starting point for the determination of $\alpha(t,t_o)$ is the time dependent form of the density matrix given by Eq. (6-14). The Hamiltonian used in Eq. (6-14) is the Hamiltonian for molecules in the presence of radiation and is given by Eq. (6-19). Combining these two equations yields the expression

$$i\hbar\dot{\rho} = (H^o\rho - \rho H^o) + (V\rho - \rho V)\cos\omega t. \tag{6-29}$$

Introduction of a basis set consisting of eigenfunctions of H^o leads to the equation

$$i\hbar\dot{\rho}_{ab} = \hbar\omega_{ab}\rho_{ab} + \sum_k (V_{ak}\rho_{kb} - \rho_{ak}V_{kb})\cos\omega t, \tag{6-30}$$

where $\hbar\omega_{ab} = E_a^o - E_b^o$. (6-31)

Here E_a^o and E_b^o are the energies of the active levels a and b and are also eigenvalues of H^o. Introduction of a set of C_{ab}, such that

$$\rho_{ab} = C_{ab}\exp(-i\omega_{ab}t), \tag{6-32}$$

followed by substitution of this expression into Eq. (6-30), limited by the restrictions of assumption (b) given in Section 6.2, yields a set of only four nonzero C_{ab}. These nonzero C_{ab} are

$$2i\hbar\dot{C}_{aa} = V_{ab}C_{ba}e^{i\delta t} - C_{ab}V_{ba}e^{-i\delta t}, \tag{6-33}$$

$$2i\hbar\dot{C}_{bb} = V_{ba}C_{ab}e^{-i\delta t} - C_{ba}V_{ab}e^{i\delta t}, \tag{6-34}$$

$$2i\hbar\dot{C}_{ab} = V_{ab}e^{i\delta t}(C_{bb} - C_{aa}), \tag{6-35}$$

and $$2i\hbar\dot{C}_{ba} = V_{ba}e^{-i\delta t}(C_{aa} - C_{bb}), \tag{6-36}$$

where $$\delta = \omega - \omega_{ba} \tag{6-37}$$

and it is assumed that $\omega_{ba} > 0$ and $|\delta| << \omega_{ba}$. The definition

$$\Delta = C_{aa} - C_{bb} = \rho_{aa} - \rho_{bb} \tag{6-38}$$

leads to the expressions

$$i\hbar\dot{\Delta} = (V_{ab}C_{ba}e^{i\delta t} - C_{ab}V_{ba}e^{-i\delta t}), \tag{6-39}$$

$$2i\hbar\dot{C}_{ab} = -V_{ab}e^{i\delta t}\Delta, \tag{6-40}$$

and $$2i\hbar\dot{C}_{ba} = -V_{ba}e^{-i\delta t}\Delta\ . \tag{6-41}$$

Eqs. (6-39), (6-40), and (6-41) form a set of coupled differential equations which can be solved exactly. Differentiation of Eq. (6-39) followed by substitution for the $\dot{C}_{ab}$ from Eqs. (6-40) and (6-41) leads to an expression which when again differentiated and followed by the same substitution from Eqs. (6-40) and (6-41) gives the differential equation

$$\dddot{\Delta} + \Omega^2\dot{\Delta} = 0, \tag{6-42}$$

where $$\Omega^2 = \delta^2 + |V_{ab}|^2/\hbar^2. \tag{6-43}$$

The solution of Eq. (6-42) is

$$\dot{\Delta} = \alpha'\cos\Omega t + \beta'\sin\Omega t, \tag{6-44}$$

which can be integrated to give

$$\Delta = (\alpha'/\Omega)\sin\Omega t - (\beta'/\Omega)\cos\Omega t + \gamma, \tag{6-45}$$

where α', β', and γ are constants of integration.

Introduction of the boundary conditions imposed by the assumption that the system is in a Boltzmann distribution at time t = 0 (when the radiation is first turned on) allows the elimination of at least two of the three integration constants. From Eqs. (6-21) and (6-32) it can be seen that C_{ab} must be zero at time t = 0, which from Eq. (6-39)

implies that $\dot{\Delta} = 0$ at time $t = 0$. From Eqs. (6-21) and (6-38) it is apparent that

$$\Delta(0) = \Delta^o = \rho_a^o - \rho_b^o \ , \tag{6-46}$$

where ρ_a^o and ρ_b^o are the Boltzmann values of ρ_{aa} and ρ_{bb}, respectively. Insertion of these boundary conditions into Eqs. (6-44) and (6-45) results in the expression

$$\Delta = \Delta^o + \beta(1 - \cos\omega t), \tag{6-47}$$

where $\beta = (\beta'/\Omega)$ is the only remaining integration constant.

Substitution for Δ into Eq. (6-41) from Eq. (6-47) yields after integration

$$C_{ba} = \frac{V_{ba}}{2\hbar} e^{-i\delta t} \left[\frac{\Delta^o + \beta}{\delta} - \frac{1}{2} \left(\frac{e^{i\Omega t}}{\delta - \Omega} + \frac{e^{-i\Omega t}}{\delta + \Omega} \right) \right] + \eta \ , \tag{6-48}$$

where η is a fourth integration constant. By taking Eq. (6-39) and substituting for Δ on the left side from Eq. (6-47) and substituting for the C_{ab} on the right side from Eq. (6-48) (here $C_{ab} = C_{ba}^*$), it can be shown that the integration constant $\eta = 0$. Also, from Eq. (6-48) and the boundary conditions $C_{ba} = 0$ and $C_{ab} = 0$ at time $t = 0$, the integration constant $\beta = (\beta'/\Omega)$ is determined to be

$$\beta = -\Delta^o |V_{ab}|^2 / \hbar^2 \Omega^2 . \tag{6-49}$$

An expression for the element ρ_{ba} of the density matrix can be obtained by substitution of the value of β given by Eq. (6-49) into Eq. (6-48) and by replacing the C_{ba} and C_{ab} by their definitions given

in Eq. (6-32). This leads to the expression

$$\rho_{ba} = \frac{\Delta^o V_{ba} e^{-i\omega t}}{2\hbar\Omega^2} [\delta(1 - \cos\omega t) - i\Omega \sin\Omega t]. \tag{6-50}$$

By making the substitution

$$d_{ba} = \frac{\Delta^o}{2\hbar\Omega^2} [\delta(1 - \cos\omega t) - i\Omega \sin\omega t] \tag{6-51}$$

the expression for ρ_{ba} is simplified to the form

$$\rho_{ba} = d_{ba} V_{ba} e^{-i\omega t} \tag{6-52}$$

and the calculation of the absorption coefficient is facilitated.

By looking again at Eqs. (6-15) through (6-18) the prescription that must be followed in order to obtain the absorption coefficient is completely defined. From Eq. (6-18) the expression for the induced dipole moment is

$$\vec{p}(t) = \rho_{ba}\vec{\mu}_{ab} + \rho_{ab}\vec{\mu}_{ba}. \tag{6-53}$$

The dipole moment matrix is assumed to have no nonzero diagonal elements in the system under investigation. Eq. (6-53) may be rewritten in the form

$$\vec{p}(t) = 2\mathrm{Re}(\rho_{ba}\vec{\mu}_{ab}). \tag{6-54}$$

Substitution for ρ_{ba} from Eq. (6-52) and substitution for V_{ba} from Eq. (6-20) yields the expression

$\vec{P}$

T

lies a

$\vec{F}$

The di

three

that o

compon

$\vec{\mu}$

can be

S

result

X

Then,

α

and by

the ti

$$\vec{p}(t) = -2\mathrm{Re}(d_{ba}\vec{\mu}_{ab}\vec{\mu}_{ba} \cdot \vec{F}^{o}e^{-i\omega t}). \tag{6-55}$$

The incident radiation is chosen to be oriented such that the field lies along the z-axis; then

$$\vec{F}^{o} = F^{o}\vec{k}. \tag{6-56}$$

The dipole moment matrix element $\vec{\mu}_{ab}$ can be written in terms of the three space-fixed orthogonal unit vectors $\vec{i}$, $\vec{j}$, and $\vec{k}$. If it is assumed that only one of the three components of $\vec{\mu}_{ab}$ is nonzero, and that this component is the z component, the expression

$$\vec{\mu}_{ab}\vec{\mu}_{ba} \cdot \vec{F}^{o} = |\mu^{z}_{ba}|^{2}\vec{F}^{o} \tag{6-57}$$

can be written.

Substitution of Eq. (6-57) into Eq. (6-55) and a comparison of the resulting equation with Eq. (6-16) implies that

$$\chi = -2d_{ba}|\mu^{z}_{ba}|^{2} . \tag{6-58}$$

Then, from Eq. (6-15) it follows that

$$\alpha = \frac{-8\pi\omega N}{c} |\mu^{z}_{ba}|^{2} \mathrm{Im}(d_{ba}) \tag{6-59}$$

and by substitution for $\mathrm{Im}(d_{ba})$ from Eq. (6-51) the final expression for the time dependent coefficient for a system with no collision is obtained.

This expression is

$$\alpha = \frac{4\pi\omega}{c} |\mu^{z}_{ba}|^2 \frac{N\Delta^{o}}{\hbar\Omega} \sin\omega t. \qquad (6\text{-}60)$$

6.5 Systems With Collisions (41)

In a system where collisions are present the expression for the absorption coefficient given by Eq. (6-60) must be averaged over the molecular collisions according to Eq. (6-26). In the derivation of Eq. (6-60) it was assumed that the molecules have not seen a Boltzmann distribution for a time interval t, which in this case is the time since the radiation was first turned on. It follows then that Eq. (6-60) in its present form is valid only for molecules which have not undergone any collision. Therefore, Eq. (6-60) represents $\alpha(t,0)$. In considering the molecular collisions in Section 6.3 it was assumed that the last collision occurred at time t_o. In this case the time interval elapsed since the molecules last saw a Boltzmann distribution is given by $(t - t_o)$. Hence, $\alpha(t,t_o)$ can be obtained from Eq. (6-60) by replacing t with $(t - t_o)$ to give the expression

$$\alpha(t,t_o) = K\sin\Omega(t - t_o), \qquad (6\text{-}61)$$

where $$K = \frac{4\pi\omega}{c} |\mu_{ba}|^2 \frac{N\Delta^{o}}{\hbar\Omega} . \qquad (6\text{-}62)$$

Substitution of the expressions for $\alpha(t,0)$ and $\alpha(t,t_o)$ given by Eqs. (6-60) and (6-61), respectively, into Eq. (6-26) gives

$$\bar{\alpha}(t) = Ke^{-t/\tau}\sin\Omega t + \int_o^t e^{-(t-t_o)/\tau}\sin\Omega(t-t_o)dt_o . \qquad (6\text{-}63)$$

Integrati

gives the

for a sy

$\bar{\sigma}(t$

For

pression

Also, Eq

degenera

interest

be intro

Integration of Eq. (6-63) followed by substitution for K from Eq. (6-62) gives the final expression for the time dependent absorption coefficient for a system with collisions as follows:

$$\bar{\alpha}(t) = \frac{4\pi\omega}{c} |\mu_{ba}|^2 \frac{N\Delta^o\tau}{1+(\tau\Omega)^2} [1 - e^{-t/\tau}(\cos\Omega t - \tau\Omega\sin\Omega t)]. \quad (6\text{-}64)$$

For the "steady-state", i.e. $t \to \infty$, Eq. (6-64) reduces to the expression for $\bar{\alpha}(t)$ obtained by Karplus and Schwinger and Snyder and Richards. Also, Eq. (6-64) has been derived for active energy levels which have no degeneracies. Therefore, when degeneracies occur, as in the case of interest here, a summation over all the states contributing to $\bar{\alpha}(t)$ must be introduced.

7.1 Re

The
associa
modifie
tion.
operate
tuned-a
crystal
capable
diagram
found f

Th
resona
more,
freque
run, a
source
must b
absolu
of the
labora
one de

VII. EXPERIMENTAL

7.1 Relaxation Time System

The spectrometer, which was used to record the time resolved spectra associated with the phenomenon of rotational relaxation in gases, is a modified Hughes-Wilson type (7) with 100 kHz square wave Stark modulation. The two primary modifications are: (1) the radiation source is operated at constant frequency instead of being swept; and (2) the usual tuned-amplifier and phase-sensitive detector which follows the microwave crystal detector is replaced by a broad-banded sampling device which is capable of time-resolving the signal from the crystal detector. A block diagram of the relaxation time system used in this investigation can be found in Figure 6.

The constant frequency of the radiation source is chosen to be the resonance frequency of the absorption line under observation. Furthermore, the radiation frequency must remain within a few kHz of the resonance frequency during the time of observation for any single experimental run, a time which can be of the order of several minutes. Thus, the source must either be extremely stable over long periods of time, or it must be capable of being stabilized in some way. Also, although not absolutely necessary, the power output of the source should be at least of the order of 50 mwatts. The sources available for use in these laboratories are klystrons and BWOs. It was soon discovered that to one degree or another both types of sources suffered from long-time

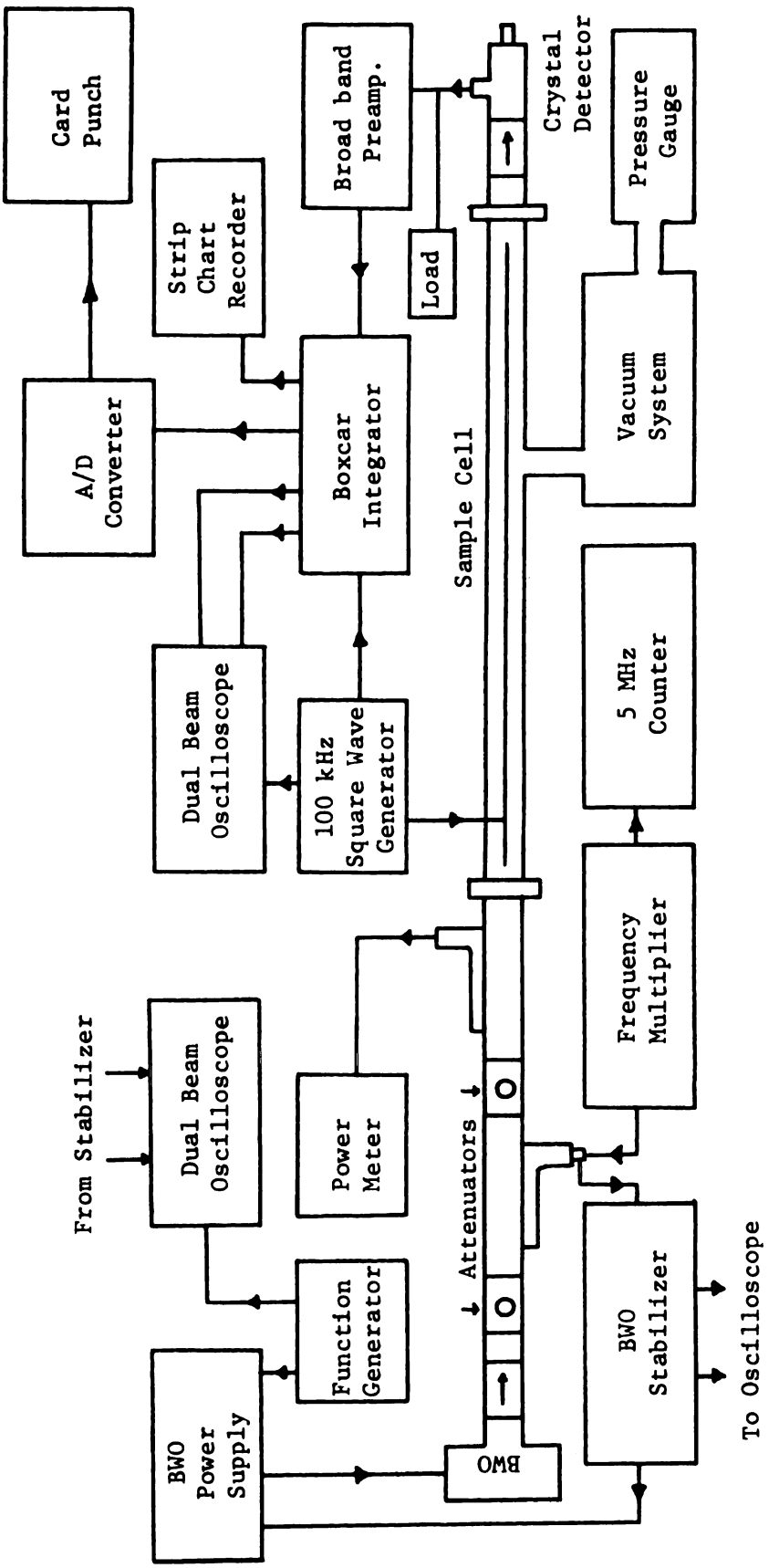

Figure 6. Block Diagram of Relaxation Time System.

instability. Therefore, it became necessary to try to stabilize these sources in some way.

Currently, source stabilization at MSU is accomplished by sampling a small portion of the radiation, mixing it with the signal from a Micro-Now Model 101c frequency multiplier, which is capable of generating harmonics of 25 MHz from a 5 MHz tunable source, and feeding the frequency difference between the source radiation and one of the harmonics into a Micro-Now Model 201c frequency stabilizer. If the frequency difference at the stabilizer is not ±60 MHz, the stabilizer sends a corrective signal to the helix electrode of the source in the case of a BWO (to the reflector electrode in the case of a klystron) to change its frequency and make the frequency difference exactly ±60 MHz. It can be seen that if the source radiation frequency is set to the resonance frequency of the line under observation and the Model 101c is tuned so that the difference frequency is ±60 MHz, it is possible to stabilize the source against small drifts. It was hoped that klystrons could be used for at least part of this investigation, because their power output is higher than that of the available BWOs, but it was not possible to stabilize them on the system being used. Thus, BWOs were used exclusively.

Just prior to entering the Stark cell the microwave radiation is sampled by means of a 20 db directional coupler and monitored with a Hewlett-Packard Model 432A power meter. Power heads for the Model 432A are available in these laboratories only for the X-band (8.0-12.0 GHz) and K-band (18.0-26.5 GHz); consequently, the investigation was limited to these frequency regions. The power levels used in the experiments ranged from about 5-50 mwatts. This is the limit of the power available in K-band, but the X-band limit is approximately 100 mwatts.

The sample cell consists of a 12 ft. piece of X-band waveguide with a Stark septum running the full length. A cell of this length provides a strong absorption signal which proved to be very beneficial in these experiments. The sample cell is joined to a vacuum system which was used for sample introduction and which also served the special purpose of providing a ballast for the sample cell. For many molecules, at the low pressures used, the pressure in the sample cell was not constant because of absorption of the molecules on the walls of the cell; therefore, it was necessary to affix a glass bulb (of 12 liters volume in the present case) to the vacuum system to stabilize the pressure in the sample cell. The cell is connected to an MKS Baratron Type 77 pressure meter which was used to determine the pressure of the gas in the cell. The Baratron is a capacitance manometer which is capable of determining absolute pressures. The range of pressures covered in this study was 8-80 mtorr, with the pressures above 50 mtorr limited to the investigation of the OCS $0 \rightarrow 1$ line in the X-band region. All experiments were carried out at room temperature.

In Chapter VI reference was made to turning the incident radiation off and on. In these experiments the radiation was not actually turned off and on but was switched in and out of resonance with the rotational energy levels by shifting the energy levels with the aid of the 100 kHz Stark modulation voltage. Normally, the incident radiation comes into resonance with the frequency of the transition when the Stark field is switched off. This corresponds to turning on the radiation. When the Stark field is switched on, the energy levels of the transition are split into their individual Stark components, which have transition frequencies differing from the main line, and consequently are no longer

in resonance with the incident radiation. Switching on the Stark field corresponds to turning off the radiation. From the above discussion, it can be seen that both the main line and the Stark components can be studied separately by a simple change in the frequency of the incident radiation if the proper half of the Stark modulation cycle is monitored.

The absorption signal from the sample cell passes through an isolator (to prevent reflections) and strikes a silicon crystal detector which rectifies the a-c component of the signal for subsequent amplification. A low-resistance load resistor connected to the crystal provides a return to ground for the crystal current. If this resistor is not chosen correctly the absorption signal may be distorted or lost. To insure that the crystal detection system is not influencing the reproducibility and quality of the signal being monitored, the following check is made whenever changes in the crystal are made. A low-voltage square wave is placed on the helix of the BWO which results in a small modulation of the output frequency of the BWO. A wavemeter is then adjusted such that the linear portion of the absorption curve resulting from power lost in the cavity is coincident with the two frequencies resulting from the square wave modulation. The resulting signal at the detector should be a square wave which looks like the modulation square wave. The modulation square wave and the resultant square wave detected at the crystal are then compared on a dual beam oscilloscope to determine the quality of the response of the detection system. The results of such a comparison can be seen in Figure 7.

The signal from the crystal detector is amplified by a factor of 100 by means of a Tektronix Model 1121 amplifier, and passed through a high-pass filter to a PAR Model 160 Boxcar Integrator (which is

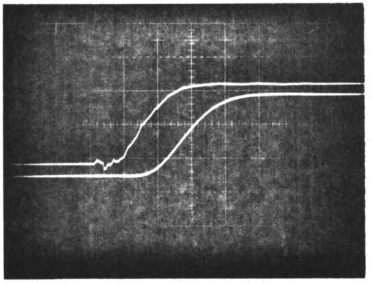

Time Scale = 0.2 μsec/division

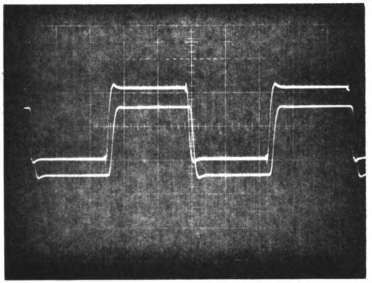

Time Scale = 2.0 μsec/division

Figure 7. A Comparison Showing the Reproducibility of the Square Wave Signal Placed on the Helix of the BWO (upper trace of both figures) with the Output of the Preamplifier of the Boxcar Integrator (lower trace of both figures).

discussed in the following section). The time variation of the raw spectrum is continuously monitored by a dual beam oscilloscope. The integrated spectrum is traced on a strip chart recorder and also stored point-by-point in a Varian C-1024 Time Averaging Computer (often referred to as the CAT). In the mode used here the CAT serves simply as an A/D converter. The storage from the CAT is then punched into cards by means of an IBM Model 526 printing summary punch.

7.2 Boxcar Integrator

The PAR Model 160 Boxcar Integrator (BI) is a high-resolution sampling and averaging device capable of extracting synchronous waveforms from noise. The BI repeatedly samples the input signal with a variable width window and variable delay gate. The delay gate can be fixed at any point or scanned across the input signal. The window allows a portion of the signal from each cycle to pass into a variable time constant integrator where the portions are summed. In this investigation the window was scanned slowly across the input signal. The large number of repetitions greatly improves the signal-to-noise ratio of the output, ultimately approaching the sensitivity of a phase-sensitive detector. The BI was chosen as the sampling device for these experiments because it features a wide range of time constants (both high and low resolution), apertures (window widths), and scan rates. It also has features which give it good hold time and stability during the scan time. A block diagram of the BI is shown in Figure 8. A brief description of the operation of the BI is given below.

The primary requirement for the proper operation of the BI is that

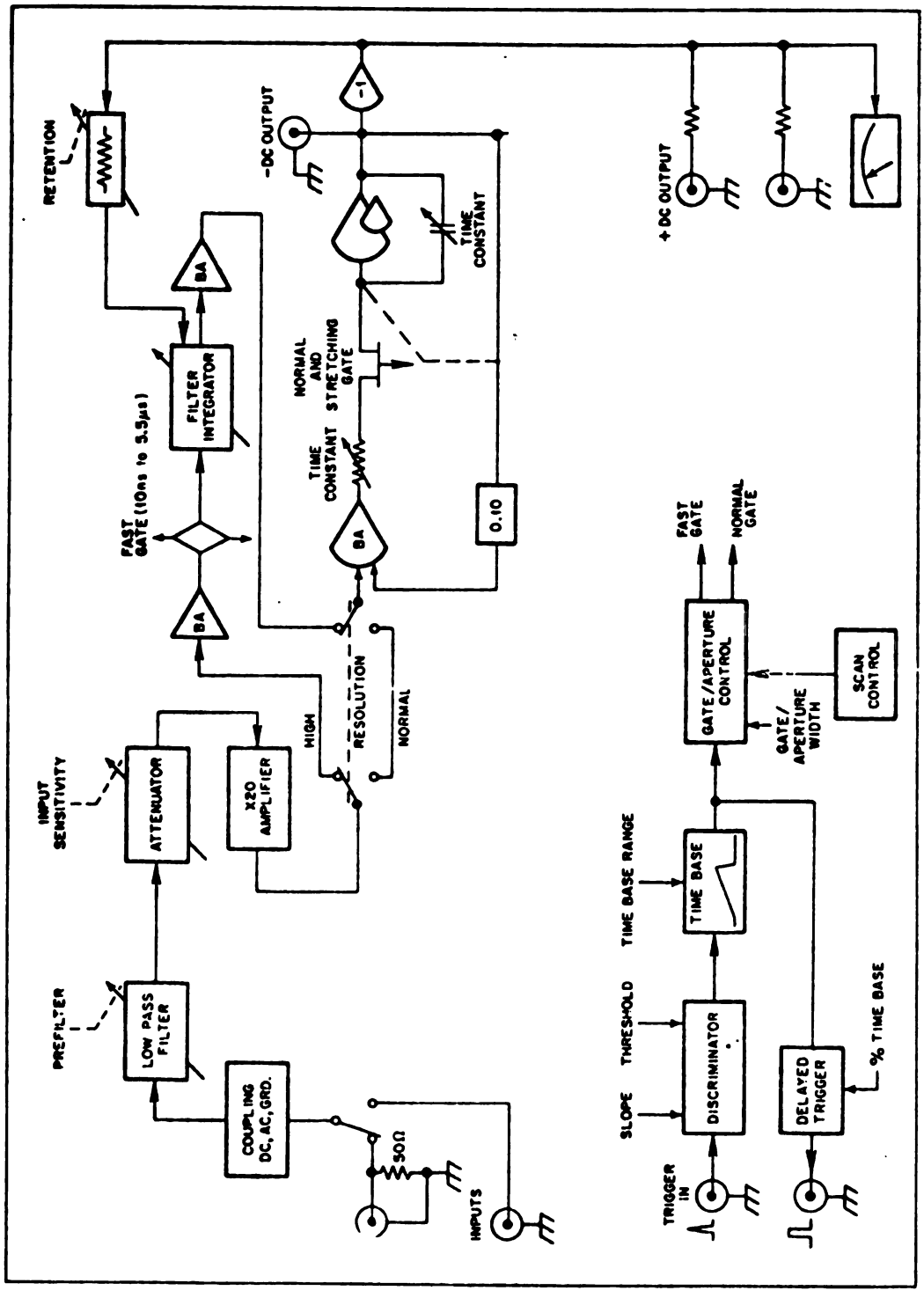

Figure 8. Simplified Block Diagram of PAR Model 160 Boxcar Integrator.

the waveform under investigation be repetitive and that a synchronizing signal, which bears a constant time relation to the waveform, precede the portion of the waveform to be studied. The "wiggle-beat" waveform is periodic as a function of the Stark modulation frequency and occurs at exactly the same point in time for each cycle of the square wave. Furthermore, a pulse from the square wave generator can serve as the trigger to initiate the scan of the Boxcar Integrator. The time base setting of the BI is determined by the modulation frequency of the square wave, which in this case is 100 kHz (i.e. 10 μsec time base). Because of the complex nature of the scanning mechanism, which does not allow every pulse from the square wave to be used, the time base must be larger than 10 μsec. For 100 kHz modulation it was found that 50 μsec was a good choice. With a time base this large, it is possible to observe several cycles of the waveform in one full scan across the time base. A pair of scan/delay dials allows the operator to set an initial starting point and final stopping point for the scan and thus provides the means for choosing the particular portion of the time base which is of interest. Thus, the actual scan may cover only 20 percent of the 50 μsec time base or 10 μsec. The scan rate can be varied by proper selection of a switch on the front panel. The obvious choice of scan rate is the fastest one which does not decrease the quality of the output signal.

The signal is filtered and preamplified (20x) before going to the integrator. The BI is capable of operating in a normal resolution mode (0.5 μsec $\leq$ aperture $\leq$ 0.55 sec) and in a high resolution mode (10 nsec $\leq$ aperture $\leq$ 5.5 μsec). The choice of mode depends on the duration of the repetitive signal, which in the present case is about 1-3 μsec. Because the width of the aperture to be scanned across the waveform can

not be greater than a very small portion of the total waveform, it is necessary to use the high resolution mode in these experiments. A convenient choice of the aperture width is one which provides good signal averaging but which at the same time does not destroy the resolution. In this case, 30 nsec proved to be a good choice. The high resolution mode of operation uses its own circuits in addition to those used by the normal resolution mode. These two sets of circuits make up the heart of the BI's operation.

In the normal resolution mode the signal from the preamplifier is sent to a buffer amplifier whose output is sent to a gating switch. This switch gates current to the summing junction of an amplifier connected as an analog integrator. Whenever the switch conducts, the circuit behaves as an integrator and whenever the switch is not conducting, the output "holds" at the last level reached while the switch was conducting. The amplifier is connected with a feedback loop such that the integrator output asymptotically approaches the average of the applied input signal. By opening the gating switch at the same time relative to each repetition of the triggered input signal, and holding it open for the same duration (aperture time) each time, the integrator output approaches the average input signal. It is the slow scanning of the gating interval across the input signal that allows the waveform to be reproduced at the output. The gating time in the normal resolution mode is slow but the "hold" characteristics are very good, which allows a very good reproduction of the input signal at the output.

In the high resolution mode, the one of interest here, the output of the preamplifier is applied to the buffer amplifier which feeds the "fast" gating switch. This mode of operation provides the gating speed

necessary to observe the waveform on the μsec time scale but provides very poor "hold" characteristics. The output of the fast gate is, therefore, integrated and held in a high-impedance buffer amplifier whose output is then slowly sent to the normal gating switch which samples the fast gate output ("stretches" it) before it can decay. A small portion of the final output signal is also sent back to the fast-gate integrator to help retain its signal level for the maximum amount of time possible. It is the time base selected, the scan/delay dial settings, and the external trigger which provide the proper timing to the gating switches allowing proper sampling of the input signal. Also, it is a combination of the time base selected, the "stretch" time, and the fly-back (scan reset) time which does not allow each trigger pulse from the square wave modulator to initiate another sampling of the waveform.

The output of the BI can be connected to a recorder and thus provide a "clean" time-resolved spectrum of the waveform being investigated. As indicated in the previous section, the signal from the BI in these experiments also provided a signal to an A/D converter which stores the signal for subsequent punching into cards.

7.3 Determination of the Time Increment

When the analog signal from the output of the BI is input into the CAT, the resulting signal becomes digitized. For a linear sweep of the CAT, the points of this digitized waveform are all separated by the same increment of time. In order to interpret the output waveform, it is necessary that this time increment be accurately known.

Initially the time increment between points on the spectrum was

obtained by scanning across one complete cycle of the modulation frequency, which is 10 μsec in duration, and then dividing this time by the total number of points in the cycle. This is an accurate method of determining the time increment but results in the collecting of about four times as many points as are useful. This method had the added disadvantage of effectively compressing the interesting portion of the waveshape into a few points, which resulted in more difficulty when trying to fit the data to the theoretical Eq. (6-64).

A method was devised whereby it is possible to obtain only that portion of the waveform of interest, while providing the needed time increment between points. The BI is set up for the waveform to be investigated, so that scanning of the BI reproduces only the interesting portion of the signal. The CAT is then set up in such a way that, when the BI and CAT are simultaneously scanned, the digitized waveform consists of approximately 100 points (100 points is all the currently used plotting routine can utilize). The time increment for any data collected with any given set of BI and CAT settings is determined as follows: (1) Adjust the frequency of a low voltage square wave generator (here a Wavetek Model 112S78) to be fast enough to produce at least one full cycle within the scanning period of the BI. (2) Apply this square wave voltage to the input of the BI and also to its triggering circuit. (3) At the same time monitor the frequency with a counter (here a Hewlett-Packard Model 5245L) so that an accurate determination of the time period for one cycle can be made. (4) Send the square wave from the output of the BI to the CAT and simultaneously scan the two. (5) Keypunch the data from the CAT into cards and calculate the time increment per point.

This method was checked for reproducibility for any given pair of settings on the BI and CAT and proved to be very reliable. Therefore, it was used exclusively in these laboratories while investigating the relaxation phenomenon.

VIII. TIME-RESOLVED SPECTRA OF CARBONYL SULFIDE AND AMMONIA

8.1 General Characteristics

The characteristics of a time-resolved spectrum can best be described by first observing the relationship of the spectrum to the square-wave modulation used to effectively turn the incident radiation off and on. This relationship for one complete period of the square-wave can be seen in Figure 9. Although the entire study was carried out using the system shown in Figure 6 of Section 7.1, the trace in Figure 9 was obtained on a Hewlett-Packard Model 8460A MRR spectrometer, which it is hoped may soon be fully adapted to these studies. The Model 8460A operates at a modulation frequency of 33 kHz; therefore, one period is 30 μsec long rather than 10 μsec which is the period for 100 kHz modulation. The absorption displayed in Figure 9 is the zero-field transition of the OCS $J = 1 \rightarrow 2$ transition.

For any zero-field transition the field-on half of the period corresponds to the radiation being turned off. During this time there should be little absorption of the radiation because the radiation frequency is not in resonance with the transitions of the Stark spectrum of the sample. The signal at the detector is then some constant value S^o which depends on the power level of the incident radiation. Ideally, S^o should be made equal for all power levels of the incident radiation to insure that the crystal responds in the same manner to each signal.

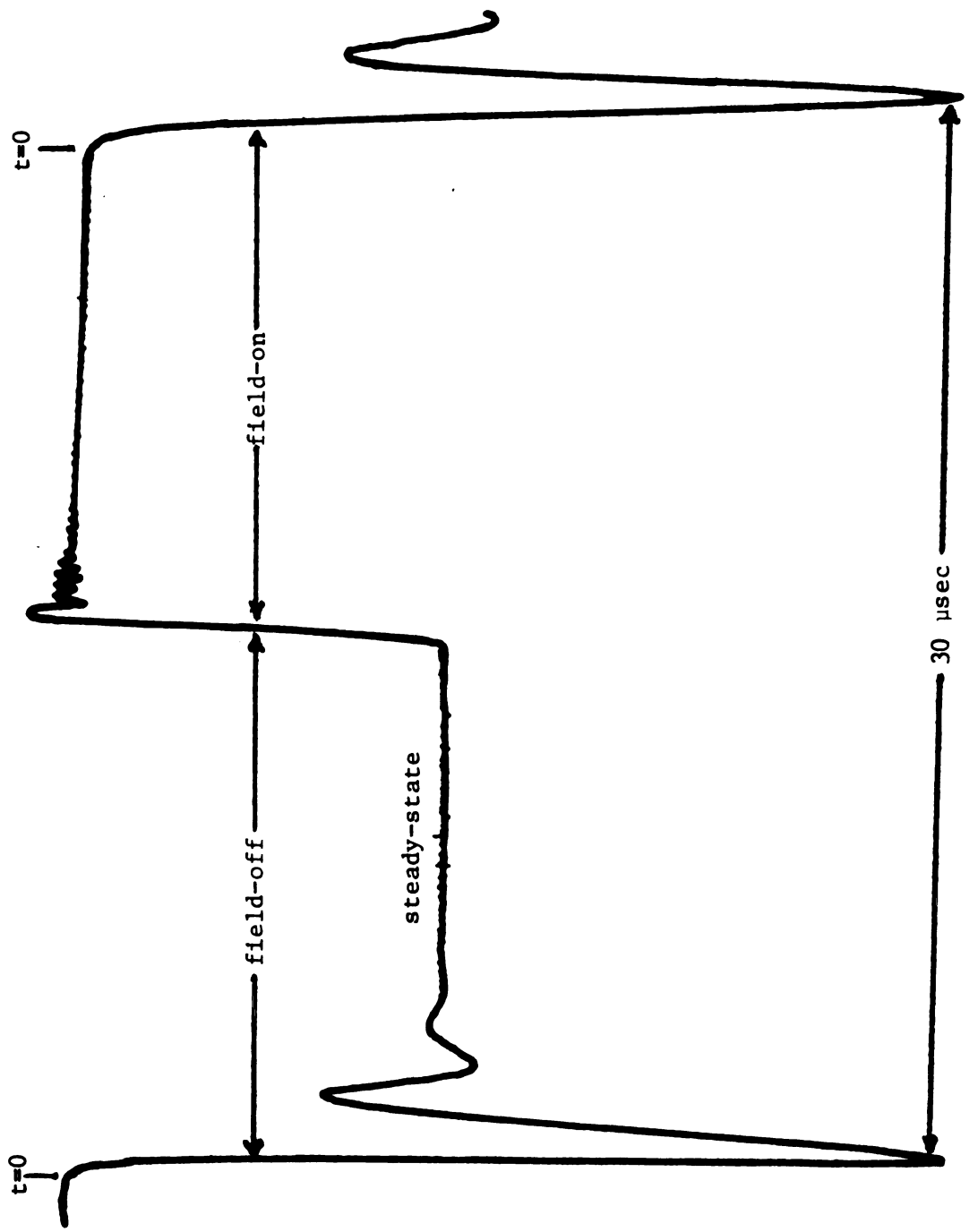

Figure 9. Trace Showing the Relationship of the "Wiggle-Beat" Line Shape to the Square Wave Modulation Field.

The easiest way to level the crystal current at differing power levels in the sample cell is to insert an attenuator before the detector. This was not done during this investigation; however, systematic variation with power of the pressure dependence of the relaxation times was observed.

When the field is turned off, the radiation comes into resonance with the zero-field transition. This corresponds to time t = 0, the time the radiation is first turned on. The signal then varies according to the time dependent absorption coefficient $\bar{\alpha}(t)$, which was derived in Chapter 6. The amplitude of the "wiggles" is damped exponentially, leaving the steady-state absorption which returns to S^o when the Stark field turns on again.

The signal at the detector may be shown to be

$$S(t) = S^o - \int_o^a \int_o^L \bar{\alpha}\,(t,P)P(x,z)dxdz\ , \qquad (8\text{-}1)$$

where $\bar{\alpha}\,(t,P)$ is the collision-averaged absorption coefficient which is a function of the time t and the microwave power P. The microwave power P(x,z) varies across the width of the cell (x = 0 to a) and down the length of the cell (z = 0 to L). This variation is assumed to be of the form

$$P(x,z) = P^o \sin^2 \frac{\pi x}{a}\, e^{-\beta z}. \qquad (8\text{-}2)$$

The integration shown in Eq. (8-1) is performed numerically; the grid has been chosen to be fine enough that a finer grid would make no significant change in S(t). The integration from 0 to a is actually

performed from d to a/2 and multiplied by two, since the power variation across the width of the cell is symmetric and since there is no gas in the region occupied by the teflon tape (of thickness d) which supports the Stark electrode.

The steady-state is reached after a time which is equal to several relaxation times. It is apparent that the more "wiggles" present in the absorption signal the better the fitting of this signal to $\bar{\alpha}(t)$ and, therefore, to Eq. (8-1).

The dependence of the absorption signal on pressure of the gas and power of the incident radiation can be seen in Figures 10 and 11. Figure 10 shows the pressure-power dependencies for the OCS J = 1 → 2 line and Figure 11 shows these dependencies for the NH_3 J,K = 3,3 line. The ability of the gaseous system to relax when perturbed by the incident radiation will be directly related to the collision rate of the molecules present. The number of collisions per unit time is dependent only on the pressure of the gas and not the power. Therefore, the relaxation time τ should vary only with pressure. This effect can be seen somewhat in Figures 10 and 11 by picking a single value for the power and observing the effect of a pressure change on the time it takes to reach the steady-state. For lower pressures the number of "wiggles" and the time to the steady-state increase for any given value of the power; i.e., there is a longer relaxation time. By looking at a series of powers for a given pressure the independence of the relaxation time on the power may be seen. Observation of such a series shows how an increased number of "wiggles" appear as the power is increased, but that an increase in the time it takes to reach the steady-state does not occur. It should also be pointed out that the steady-state amplitude decreases;

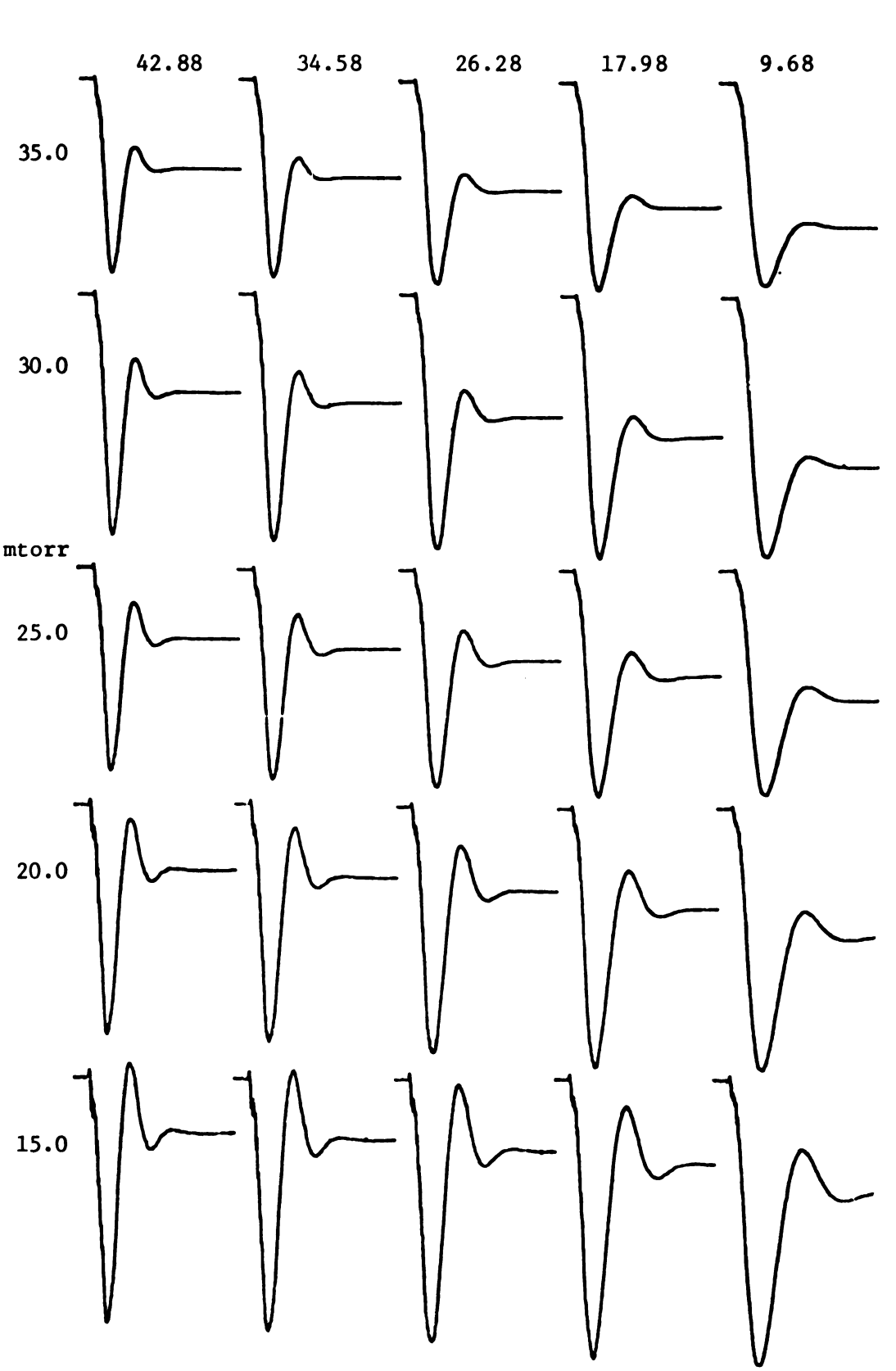

Figure 10. Pressure-Power Dependence of the "Wiggle-Beat" Spectrum for the OCS J = 1 → 2 Transition.

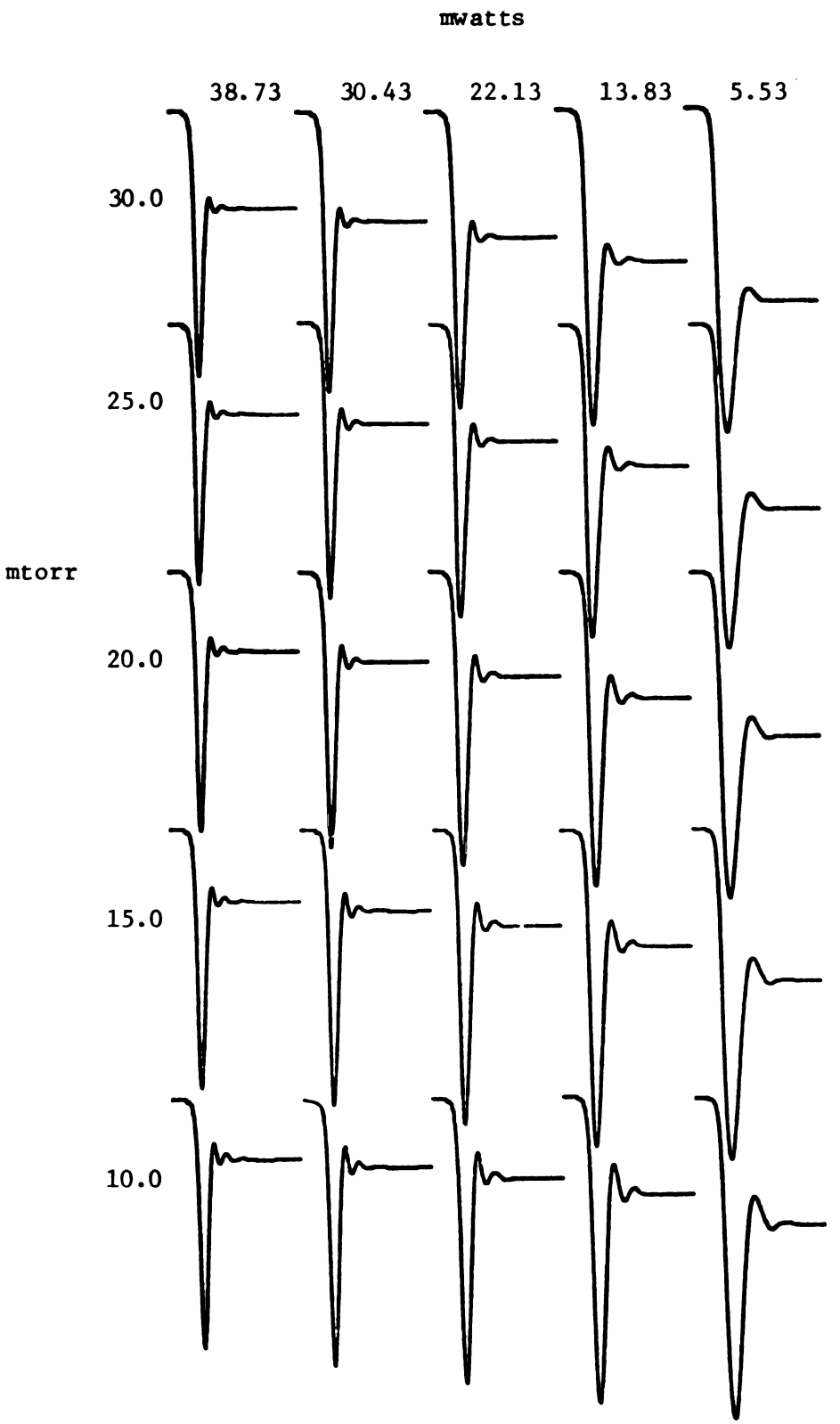

Figure 11. Pressure-Power Dependence of the "Wiggle-Beat" Spectrum for the NH_3 J,K = 3,3 Transition.

i.e., the difference between the initial non-absorption signal S^o and the steady-state signal decreases as the power increases. This is saturation; i.e., the steady-state energy level populations become more nearly equal as the power increases.

A rather unexpected and as yet unexplained phenomenon is observed when the frequency of the incident radiation is tuned slightly off the resonant absorption frequency for the transition. This phenomenon can be seen in Figures 12 and 13 for the OCS $J = 1 \rightarrow 2$ transition and the NH_3 J,K = 3,3 transition, respectively. There are three things of interest to be noted in these figures. The first and most important is that the waveforms show an asymmetry of the amplitude of the wiggles about the resonance frequency ν_o (0.0 in the figure). This asymmetry is much more pronounced in the case of the NH_3 J,K = 3,3 transition and gives a very strong signal on the high frequency side of ν_o. The $J = 1 \rightarrow 2$ transition of OCS is seen to be slightly asymmetric and also gives stronger signals on the high frequency side of ν_o. This effect follows closely the Stark pattern for each of these lines and so a check of several other lines with known Stark effects was made. In each case the pattern of the asymmetry followed the pattern of the Stark effect for the line being observed. Therefore, it is concluded that the asymmetry is most likely dependent in some way on the Stark effect. It has been suggested by Pickett (43) that this effect is due to the fact that the radiation is effectively turned on and off rather than actually being turned on and off. It is believed that a correction in the boundary conditions used to find $\alpha(t)$ (in Section 6.4) which includes the effect of the modulation field would result in an expression for $\alpha(t)$ which would predict the asymmetry.

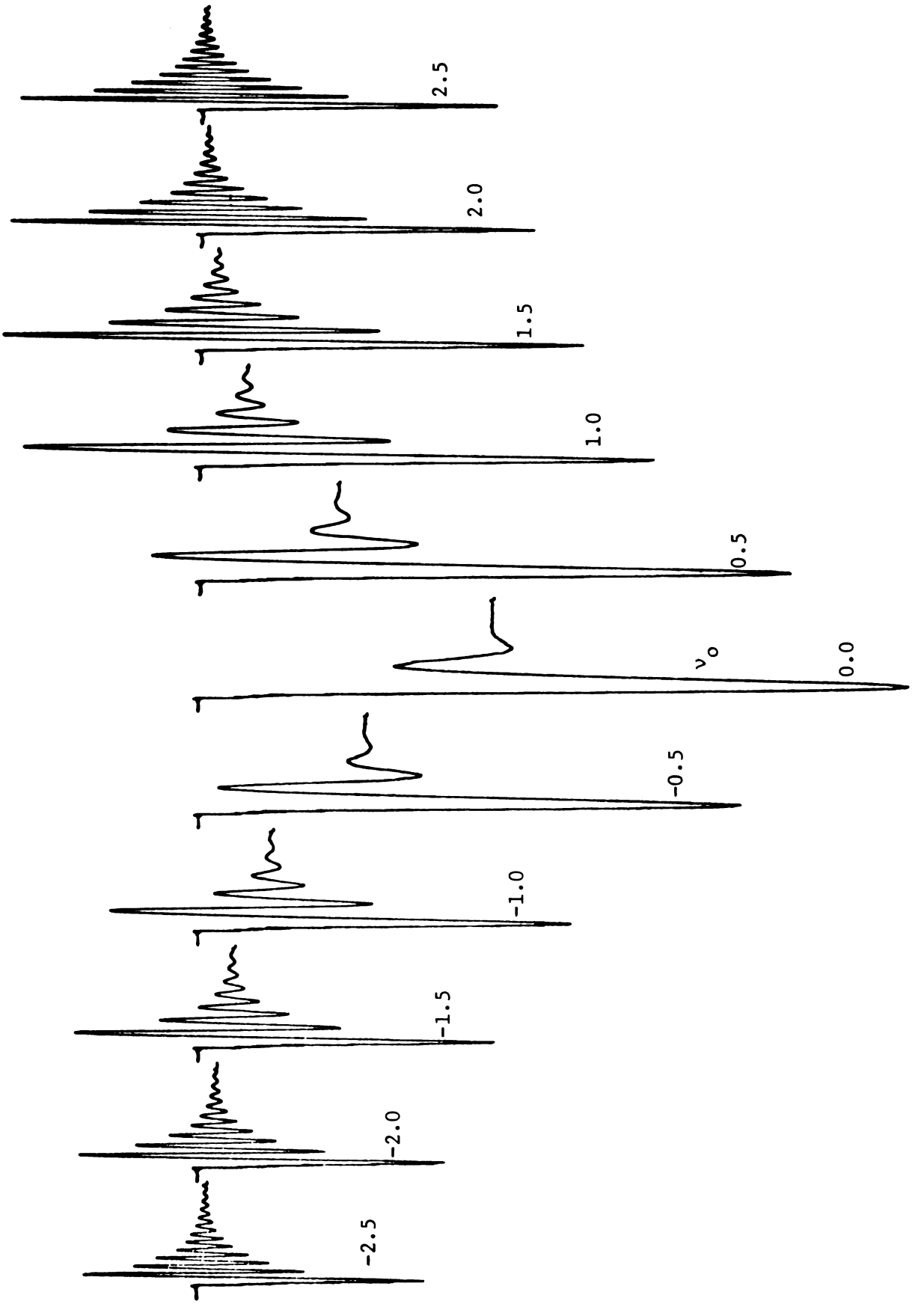

Figure 12. Off-Resonance Effect Observed in the OCS J = 1 → 2 Transition. (Shifts given in MHz.)

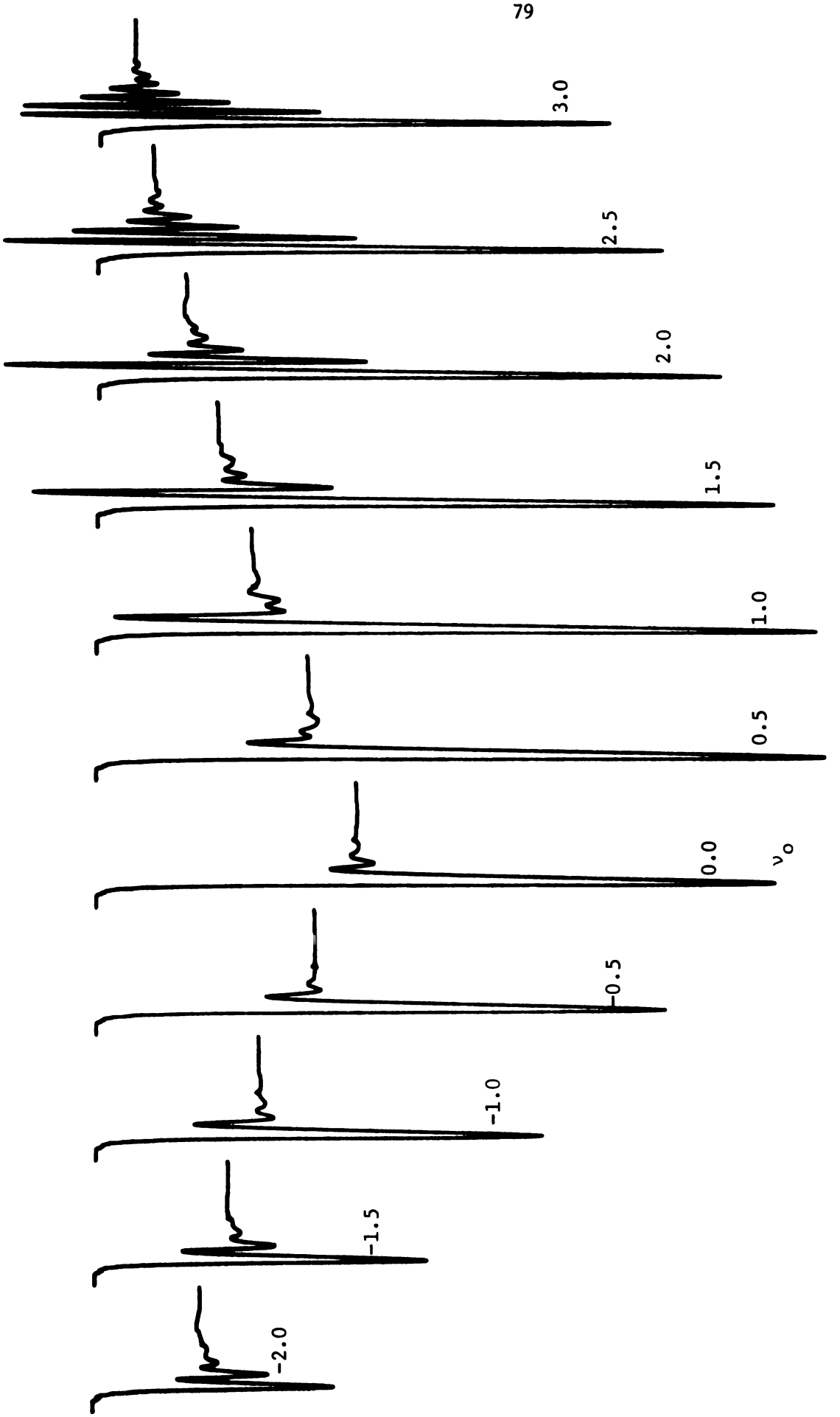

Figure 13. Off-Resonance Effect in NH_3 J,K = 3,3 Transition. (Shifts given in MHz.)

The second interesting point in Figures 12 and 13 is the increased number of "wiggles" that appear as the frequency is tuned farther and farther off-resonance. This increased number of "wiggles" may well be used to great advantage in determining the relaxation times due to the increased sensitivity of the fitting equation to this waveshape. This, however, can not be realized until an accurate $\alpha(t)$ can be derived for the off-resonance case.

The third interesting feature is that the steady-state signals for any series of off-resonance runs trace out a typical symmetric absorption pattern as seen in normal spectroscopy. These off-resonance waveshapes are easily obtained by detuning the frequency multiplier a predetermined amount so as to cause the locking of the BWO to take place at the desired off-resonance frequency.

Probably the most critical stage in any investigation such as this is to check the compatibility of the theory and the experimental data. In order to do this it was necessary to write a computer program which could take the experimental data and fit it to the theoretical expression $\overline{\alpha}(t)$ derived in Chapter 6. Professor R. H. Schwendeman wrote such a computer program using five variable parameters, one of which is the desired relaxation time parameter τ. A discussion of these fitting parameters may be found in Appendix A, and a complete set of final values obtained for these parameters resulting from the fittings may be found in Appendix B. Initial attempts to use the program indicated a need for refinements. It was discovered that the distribution of the power level in the waveguide, both across the cell and lengthwise down the cell, was not insignificant and had to be considered in the fitting. Subsequent use of this "power-averaged" version of the program in fitting

the data still indicated irregularities in the results which could not be accounted for. Further investigation showed that the dependence of the power saturation on the degenerate M states of a transition had been omitted. Insertion of this correction into the program resulted in reliable fitting of the data for all three transitions investigated during this study. The results for each of these three transitions are discussed in the following sections.

8.2 OCS J = 0 → 1 Transition

The OCS J = 0 → 1 transition was chosen because it is probably the least complex and most well known line in microwave spectroscopy. Such a line is necessary in an initial investigation to insure that a minimum of unexpected phenomena occur. Also, well-studied transitions usually have an abundance of data available for comparison.

The first attempts at fitting the data to the theoretical expression by using the computer program WBFITP3 (final corrected version) were carried out by starting the fitting at time t = 0, i.e., when the Stark field first began to turn off. Unfortunately, the resulting fits were very poor, especially in the region near t = 0. The poor fits were attributed to the large error introduced by the fall-time of the square wave (approximately 0.6 μsec). It was, therefore, necessary to choose a later starting point for the fitting. The point selected lies approximately half way between the time t = 0 and the first minimum of the "wiggle-beat" spectrum. Figure 14 shows the results of such a fitting on the OCS J = 0 → 1 transition using WBFITP3.

The plot in Figure 14 which compares the experimental points (the x's)

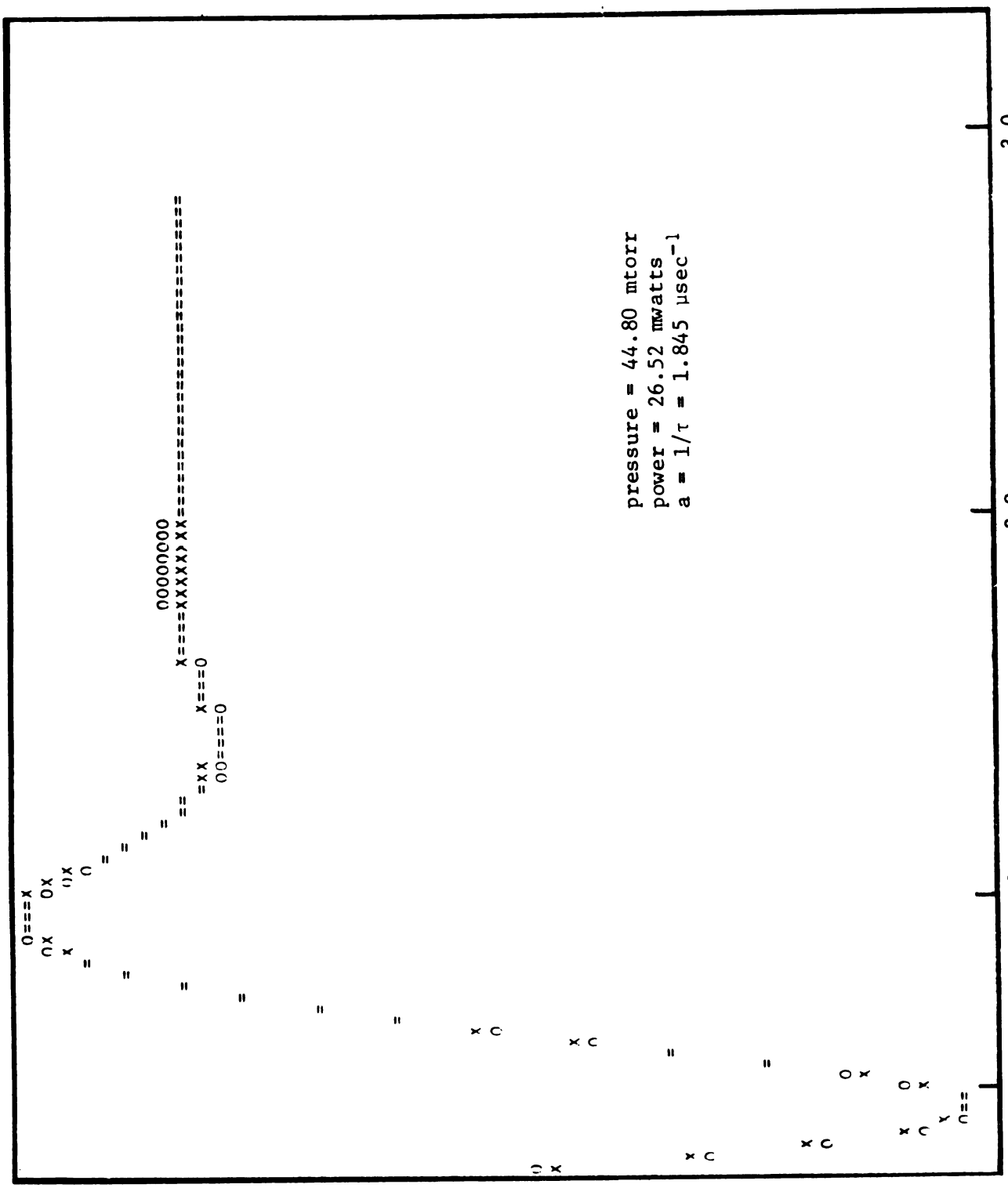

Figure 14. Typical Result of a Fitting on the OCS J = 0 → 1 Transition Using WBFITP3.

to the calculated theoretical points (the o's) is printed directly as output from the program WBFITP3. The abscissa of the plot is divided into equal time segments, one for each data point, up to a maximum of 100 points. The ordinate is divided into 50 equal segments whose magnitude depends on the maximum and minimum signals included in the fitting; therefore, each increment represents two percent of full scale. Differences between the experimental values and the calculated values along the ordinate may be used to estimate errors in the fitting. If the difference falls within one vertical increment an equal sign appears in the plot.

Each fitting, as seen in Figure 14, when made at a given power and pressure, provides a value for $a = 1/\tau$, which is the overall rate constant for rotational relaxation under particular conditions. A series of such fittings taken at different powers and pressures then gives a method of obtaining the pressure dependent contribution to the relaxation rate. The pressure dependent contribution, which should contain that part of the relaxation which is due to molecular collisions, is obtained by plotting $a = 1/\tau$ vs. pressure for any fixed value of the power. The slope of such a plot multiplied by the pressure is the pressure-dependent contribution to the relaxation rate. A typical plot of a vs. p for the OCS $J = 0 \rightarrow 1$ line can be seen in Figure 15. Because the relaxation rate should not depend on the power, a comparison of the slopes of a vs. p for any number of different powers should all be the same. Further comments on this point are made in Section 8.5.

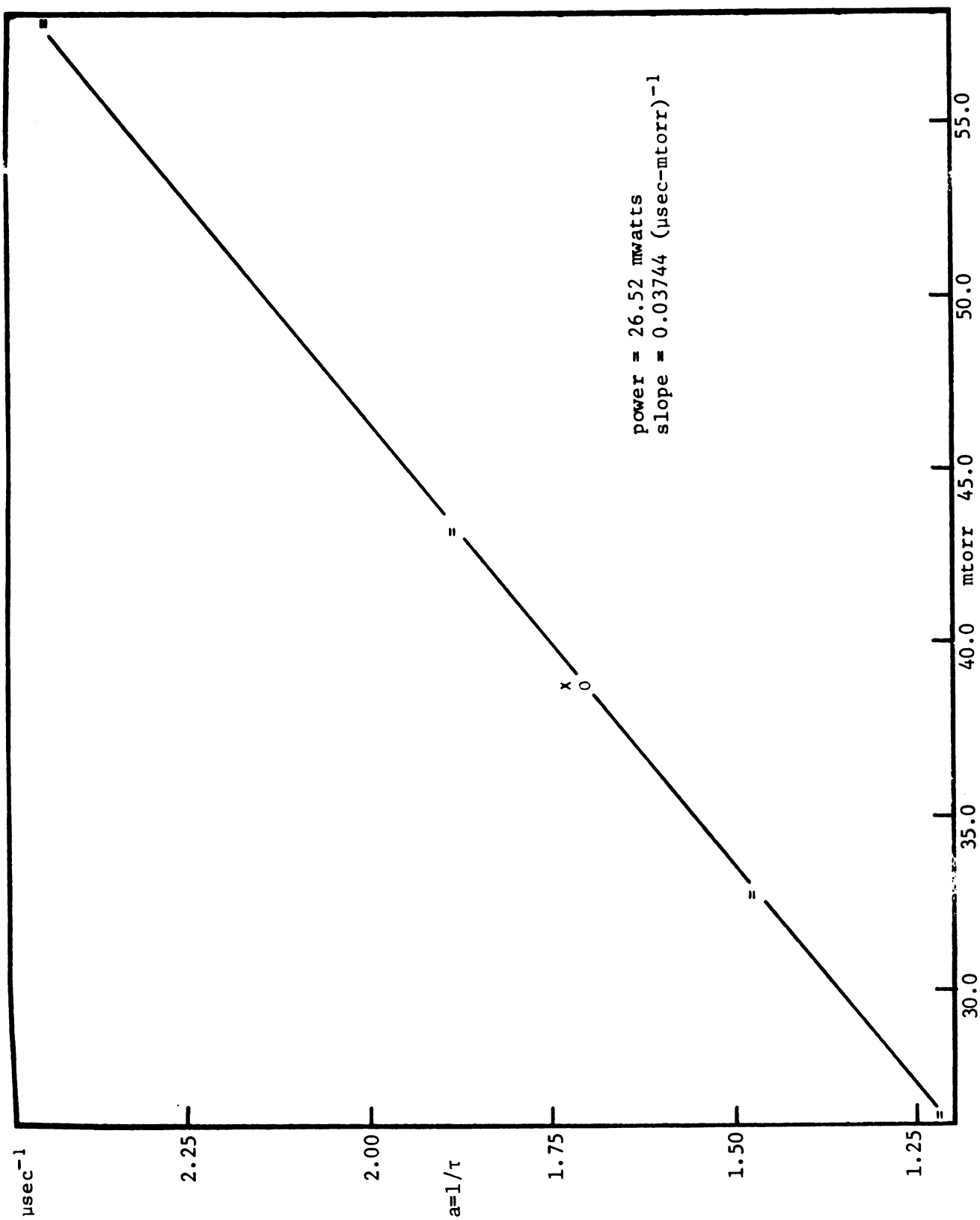

Figure 15. Typical Plot of a vs. p for the OCS J = 0 → 1 Transition.

8.3 OCS J = 1 → 2 Transition

The OCS J = 1 → 2 transition was investigated for the same reasons as the OCS J = 0 → 1 transition. The most important difference between these two transitions is the occurrence of two Stark components in the J = 1 → 2 transition whereas the J = 0 → 1 has only a single Stark component. Therefore, this is the first transition studied which showed the effects of the summation over the degenerate states mentioned in Section 8.1. The results for the J = 1 → 2 transition are essentially the same as those for the J = 0 → 1 transition and can be seen in Figures 16 and 17. Figure 16 shows a typical fitting for the OCS J = 1 → 2 transition using the program WBFITP3 and Figure 17 gives an example of a typical plot of a vs. p for this transition. A comparison of the results for the J = 1 → 2 transition with the results for the J = 0 → 1 transition will be given in Section 8.5.

8.4 NH_3 J,K = 3,3 Transition

The NH_3 J, K = 3,3 transition, which is the result of a transition between the two levels of an inversion doublet, was probably the most difficult yet most interesting transition studied during this investigation. It was this transition, which has three Stark components, which pointed out the limitations of failing to sum over the degenerate M states of a transition. It was not until this summation was introduced that a fitting on this transition could be made with any reliability. The relaxation rate for this transition was found to be about five times faster than that for either of the two OCS transitions. Therefore, it was necessary to work at lower pressure ranges in order to see any marked effect due to power variations. This increase in the relaxation rate is due to the

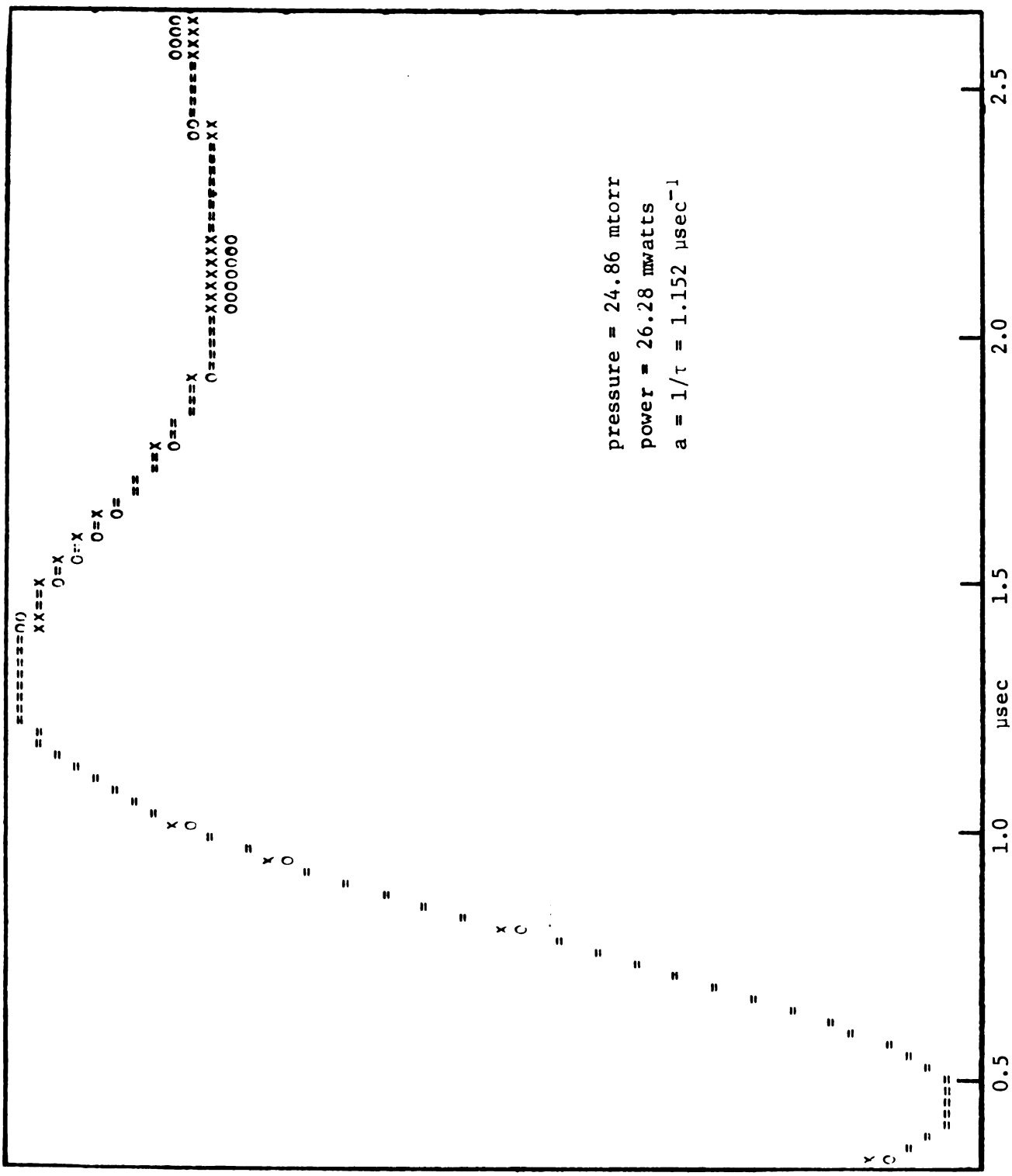

Figure 16. Typical Result of a Fitting on the OCS J = 1 → 2 Transition Using WBFITP3.

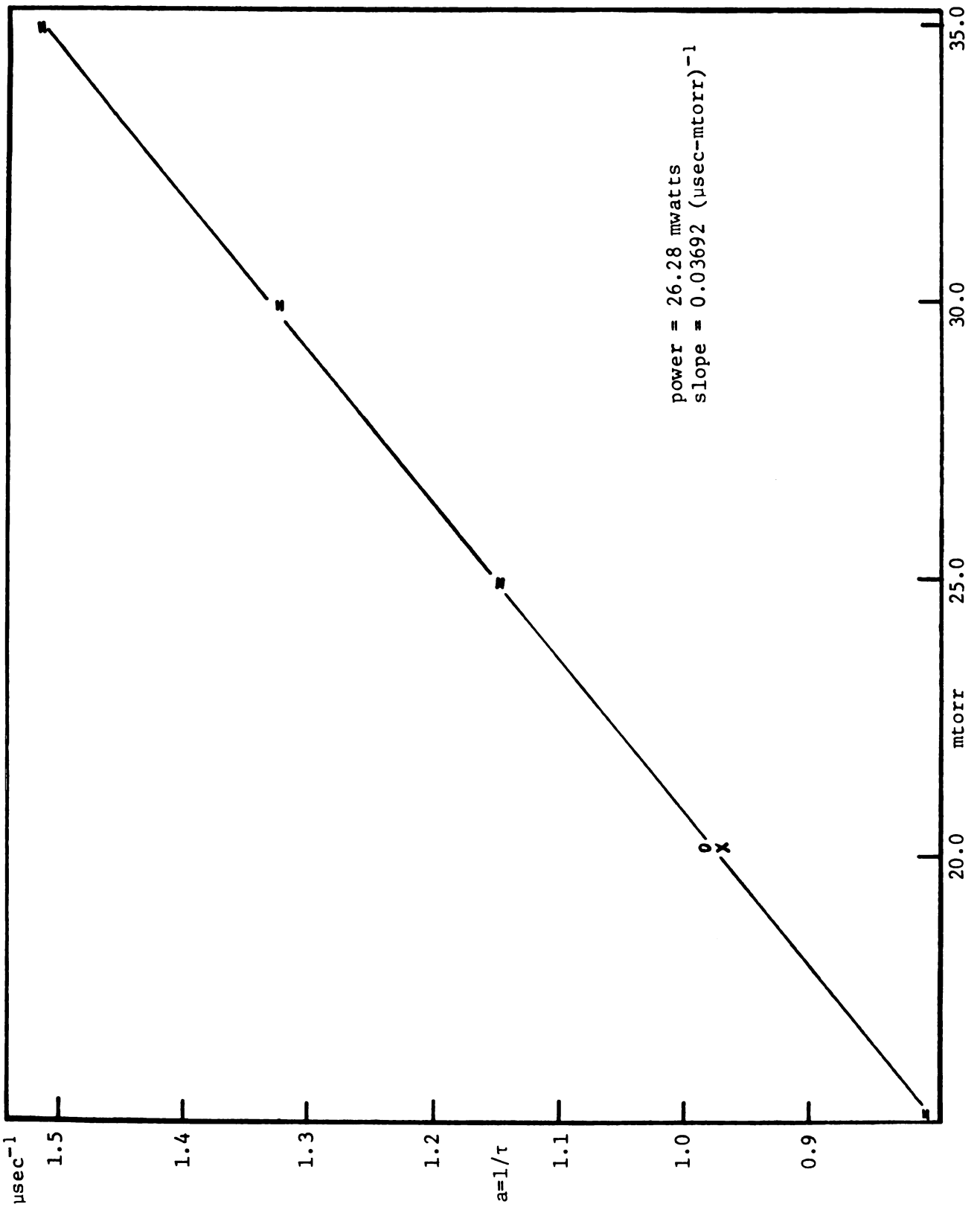

Figure 17. Typical Plot of a vs. p for the OCS J = 1 → 2 Transition.

faster velocity of the NH_3 molecules (smaller τ) and the larger effective diameter for collisions. Also, the absorption coefficient depends on the dipole moment of the gas under investigation, as seen in Eq. (6-64), and is about twice as large in NH_3 as it is in OCS. The results of a typical fitting on the NH_3 J,K = 3,3 transition using WBFITP3 is given in Figure 18. The much shorter time scale indicates that a shorter time is needed to reach the steady-state. Figure 19 shows a typical plot of a vs. p for the NH_3 J,K = 3,3 line. It was found that the relaxation times obtained for high pressures deviated from the straight lines defined by the relaxation times for the lower pressures. This effect will be discussed in the next section.

8.5 Discussion

A summary of the pressure dependent rotational relaxation rate constants (slopes of a vs. p) obtained at various powers of the incident radiation for each of the three transitions studied during this investigation is given in Table VII. It can be seen that there are two columns of figures for each transition. The columns marked "Initial" are the results obtained when all the experimental points are used. It can be seen that these values for the slopes vary considerably and irregularly with a change in power. Therefore, the plots from the slope calculations were used to determine if any of the points deviated far enough from the line to justify omitting them from the calculations. In the case of the two OCS transitions several such possibilities occurred and new slopes were calculated in these cases. In the case of the NH_3 transition it was found that the high pressure points all seemed to be too large

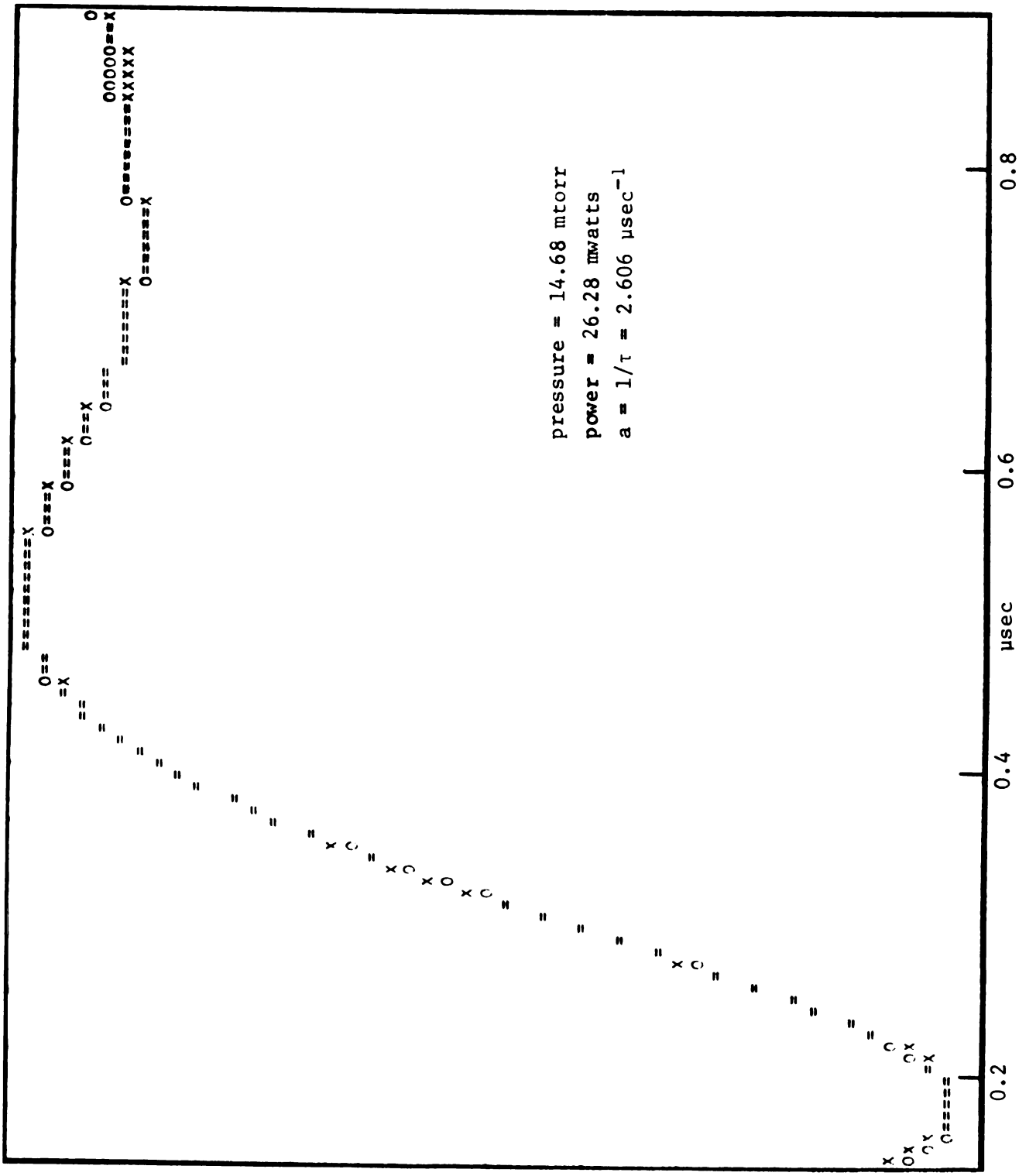

Figure 18. Typical Result of a Fitting on the NH_3 J,K = 3,3 Transition Using WBFITP3.

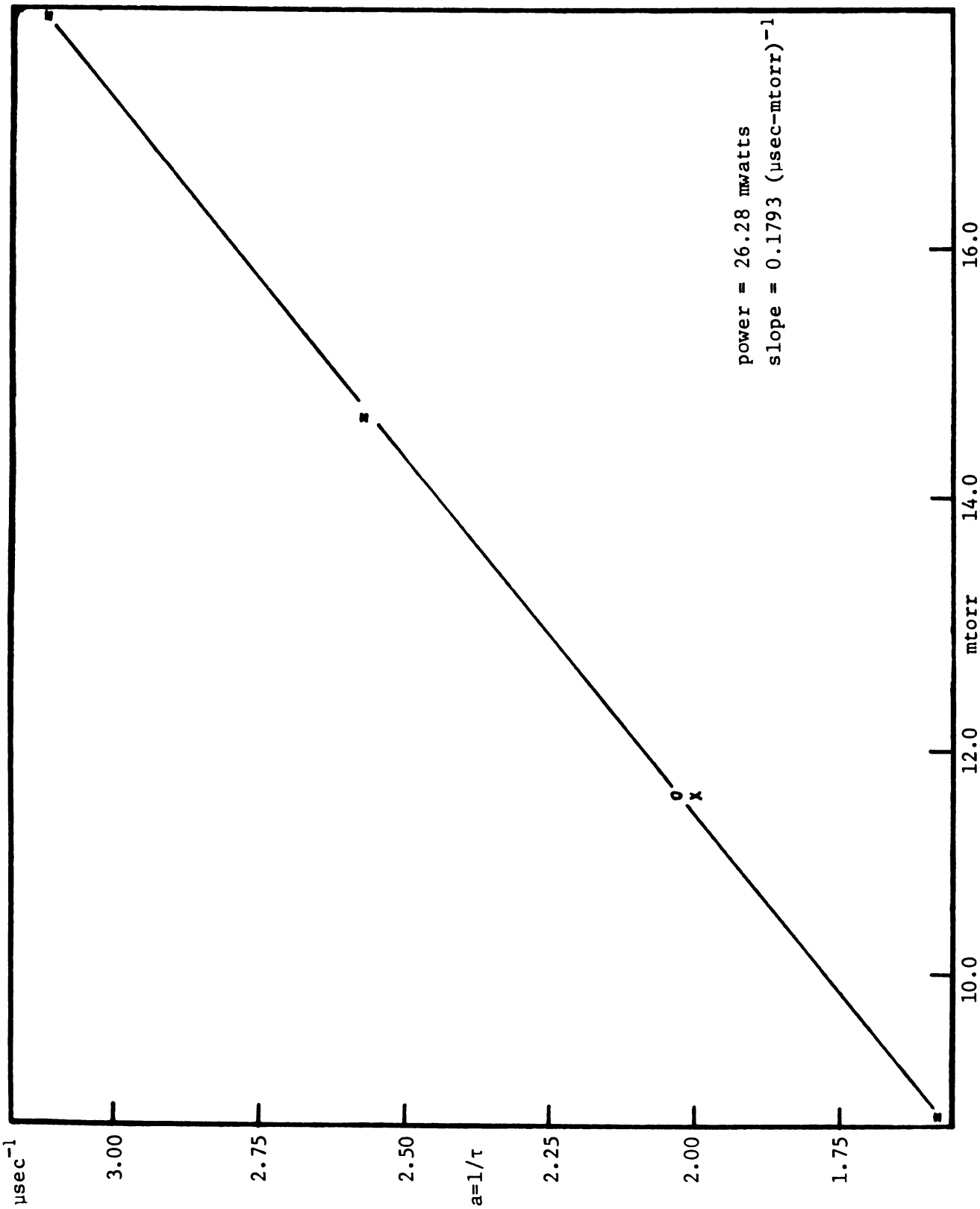

Figure 19. Typical Plot of a vs. p for the NH_3 J,K = 3,3 Transition.

Table VII. Experimental Slopes[a] Obtained from Plots of a vs. p for Various Powers[b] of the Incident Radiation.

	OCS J=0→1			OCS J=1→2		NH_3 J,K=3,3	
Power	Initial	Final	Power	Initial	Final	Initial	Final
51.61	0.03655	0.03747	38.73	0.03805	0.03617		
44.88	0.03396	0.03378	34.58	0.04506	0.03811	0.1985	0.1819
38.76	0.03549	0.03540	30.43	0.04646	0.04398	0.2052	0.1922
32.64	0.03655	0.03655	26.28	0.03692	0.03692	0.2059	0.1793
26.52	0.03997	0.03744	22.13	0.03861	0.03861	0.1960	0.1843
20.40	0.04230	0.04230	17.98	0.03709	0.03709	0.1869	0.1808
15.30	0.03710	0.03710	13.63	0.03656	0.03475	0.1720	0.1687
10.20	0.04051	0.04051	9.68	0.03602	0.03539	0.1566	0.1685
	(0.03780)[c]	(0.03757)		(0.03935)	(0.03763)	(0.1887)	(0.1794)
$(p\tau)^{d}$=	26.45	26.62	$p\tau$=	25.42	26.58	5.299	5.575

[a] In $(\mu sec\text{-}mtorr)^{-1}$. Initial values obtained with raw experimental data; final values obtained after consideration of possible bad points.

[b] In mwatts.

[c] Values in parentheses are averages.

[d] $p\tau$ = (average slope)$^{-1}$ in μsec-mtorr.

and so all these points were left out of the slope calculations. The new slopes obtained after these data omissions are those found in the columns labeled "Final". It is apparent that the changes in slope as a result of the data omissions are very small for OCS, but of the order of five percent for NH_3. Considering the fact that the original fittings on the data using the program WBFITP3 indicated differences between the experimental and theoretical points of only about two percent, it is quite disappointing to have variations of up to 15 percent in the slope calculations.

A check of the standard deviation for the fitting parameter $a = 1/\tau$ in each of the experimental runs was made to determine if the magnitude of the deviations could be correlated to the variations in the slopes. There appeared to be no detectable relationship between the two. However, since provisions for maintaining a constant crystal current at varying power levels were not available at the time of this investigation, it is suspected that the variations in the slopes may be due in part to a nonuniform response of the crystal detector to changes in power level. The desired relaxation rate constant for each of the transitions studied was taken to be an average of the slopes listed in Table VII.

Pressure dependent effects on a transition are usually discussed in terms of linewidths. The linewidth is related to the mean time between collisions τ by the equation

$$\Delta\nu = 1/2\pi\tau, \tag{8-3}$$

where $\Delta\nu$ is the half-width at half-height for the transition. The τ associated with the normal linewidth, which is described by the Lorentz line shape, can be found in Eq. (6-64) as part of the time independent

coefficient preceding the bracketed quantity. The τ used to obtain the values of the slopes in the relaxation studies done here appears in the exponential damping factor found within the bracketed quantity of Eq. (6-64). The fittings were done using only the "exponential" τ as a fitting parameter. This experimental τ is termed a relaxation τ because of the way it appears in Eq. (6-28), which casts it in an equilibrium-restoring perspective.

The relationship of the two τ's to the linewidth and to each other has been worked out by Schwendeman (41) based largely on suggestions by Oka. If the linewidths are written in terms of the rate constants for transitions of the molecules between the active energy levels E_a and E_b, and transitions between these levels and any of the other levels, the following expressions are obtained:

$$\Delta\nu_{\ell} = \frac{(k_{ab} + k_{ba})}{2} + \sum_{j} \frac{(k_{aj} + k_{bj})}{2} \tag{8-4}$$

and

$$\Delta\nu_{r} = (k_{ab} + k_{ba}) + \sum_{j} \frac{(k_{aj} + k_{bj})}{2} . \tag{8-5}$$

The constant k_{ab} is the rate constant for transitions from level a to level b, k_{aj} is a rate constant for transitions from level a to level j, etc., where the j levels represent all the remaining levels (i.e., excluding levels a and b). It is possible to combine Eqs. (8-4) and (8-5) into the following expression:

$$\Delta\nu_{r} = \Delta\nu_{\ell} + \frac{(k_{ab} + k_{ba})}{2} . \tag{8-6}$$

Table VIII compares the linewidths obtained from linewidth measurements with those obtained from the relaxation studies. It can be seen that the values of the linewidths calculated for the OCS J = 0 → 1 and the OCS J = 1 → 2 transitions from the relaxation studies are essentially the same as those obtained from previous studies. On the other hand, the NH_3 J,K = 3,3 linewidth obtained by relaxation techniques is larger than that found previously. The implications of these results can be determined by referring to Eqs. (8-4) and (8-5) and comparing terms in these expressions. It is readily apparent that the only difference between the two expressions is a factor of 1/2 in the first term. Therefore, if the linewidth is largely dependent on the transitions between the active energy levels a and b, the value of the linewidth for the relaxation experiments should be twice as large as that obtained from normal linewidth measurements. On the other hand, if the important contribution comes from transitions to energy levels other than levels a and b, the value of the linewidth obtained from relaxation experiments should be the same as that obtained from normal linewidth measurements.

The molecule OCS has available many closely spaced rotational energy levels and affords a large reservoir which permits relaxation to take place without a large dependence on transitions between the active levels a and b. Therefore, it would be suspected that the linewidths obtained for OCS from relaxation studies would be similar, but slightly larger than those obtained from normal spectroscopy. However, in the NH_3 molecule the inversion doublets are widely spaced and hence the relaxation must depend heavily on transitions between the active levels a and b. Therefore, the linewidth from relaxation studies should be nearly a factor of two larger than that obtained from normal linewidth measurements.

Table VIII. Comparison Between Linewidths[a] Obtained from Relaxation Studies and Those Obtained from Standard Linewidth Measurements.

Transition	Relaxation[b]	Line Width	Reference
OCS J=0→1	6.02	6.05[c]	(52)
	5.98		
OCS J=1→2	6.26	6.28[c]	(52)
	5.99	6.0	(53)
		6.1	(54)
		6.1	(55)
		6.4	(56)
		6.27	(57)
NH_3 J,K=3,3	30.0	27.0	(58)
	28.6	30.0	(59)
		24.0[c]	(60)
		25.7	(61)

[a] In MHz/torr.

[b] First value given for each transition is calculated from "Initial" slopes in Table VII and second value is calculated from "Final" slopes.

[c] Most recent measurement.

When compared to previous studies, the linewidths obtained in this investigation are only 20 percent larger in the case of NH_3 and practically identical in the case of OCS. It is apparent that further investigation of the relaxation phenomenon in other molecular systems is necessary before any concrete conclusions can be drawn.

REFERENCES

REFERENCES

1. H. H. Nielsen, Phys. Rev., 40, 445 (1932).
2. C. E. Cleeton and N. H. Williams, Phys. Rev., 45, 234 (1934).
3. B. Bleaney and R. P. Penrose, Nature, 157, 339 (1946).
4. D. K. Coles and W. E. Good, Phys. Rev., 70, 979L (1946).
5. T. W. Dakin, W. E. Good, and D. K. Coles, Phys. Rev., 70, 560L (1946).
6. Ibid., 71, 640L (1947).
7. R. H. Hughes and E. B. Wilson, Jr., Phys. Rev., 71, 562L (1947).
8. W. C. Michaels and N. L. Curtis, Rev. Sci. Instr., 12, 444 (1941).
9. R. V. Pound, Rev. Sci. Instr., 17, 490 (1946).
10. H. N. Volltrauer and R. H. Schwendeman, J. Chem. Phys., 54, 260 (1971).
11. Ibid., p. 268.
12. P. L. Lee, and R. H. Schwendeman, J. Mol. Spec., 41, 84 (1972).
13. E. G. Codding, Ph.D. Thesis, Michigan State University, 1971.
14. E. B. Wilson, Jr. and J. B. Howard, J. Chem. Phys., 4, 260 (1936).
15. D. R. Herschbach and V. W. Laurie, J. Chem. Phys., 37, 1668 (1962).
16. J. E. Wollrab, Rotational Spectra and Molecular Structure, Academic Press, New York, 1967, pp. 7-8.
17. H. Erying, J. Walter and G. E. Kimble, Quantum Chemistry, John Wiley and Sons, Inc., New York, 1944, p. 39.
18. Ibid., p. 41.
19. Reference 16, p. 12.
20. G. W. King, R. M. Hainer, and P. C. Cross, J. Chem. Phys., 11, 27-42 (1943).

21. S. C. Wang, Phys. Rev., 34, 243 (1929).

22. W. Gordy, W. V. Smith, and R. F. Trambarulo, Microwave Spectroscopy, Dover Publications, Inc., New York, 1966, pp. 116-18.

23. C. H. Townes and A. L. Schawlow, Microwave Spectroscopy, McGraw-Hill Book Company, New York, 1955, Sections 10-1 and 10-2.

24. Reference 16, Chapter 8.

25. For more information on the 8460A write Hewlett-Packard, Palo Alto, California.

26. Reference 16, Chapter 9.

27. Reference 22, Chapter 1.

28. H. N. Volltrauer, Ph.D. Thesis, Michigan State University, 1970.

29. P. L. Lee, Ph.D. Thesis, Michigan State University, 1971.

30. Reference 13, Chapter 3.

31. J. S. Muenter, J. Chem. Phys., 48, 4544 (1968).

32. R. Assink was an undergraduate honors student working under the direction of Professor R. H. Schwendeman.

33. T. E. Turner and J. A. Howe, J. Chem. Phys., 24, 924 (1956).

34. Handbook of Chemistry and Physics, The Chemical Rubber Co., Cleveland, 45th Edition, F-93 (1964).

35. A. L. McClellan, Table of Experimental Dipole Moments, W. H. Freeman and Company, San Francisco, (1963).

36. J. H. Hand, Ph.D. Thesis, Michigan State University, 1965.

37. J. H. Van Vleck and W. F. Weisskopf, Rev. Mod. Phys., 17, 227 (1945).

38. P. W. Anderson, Phys. Rev., 76, 647 (1949).

39. R. Karplus and J. Schwinger, Phys. Rev., 73, 1020 (1948).

40. H. S. Snyder and P. I. Richards, Phys. Rev., 73, 1178 (1948).

41. R. H. Schwendeman. Michigan State University, East Lansing, Michigan, to be published.

42. H. W. Harrington, Symposium on Molecular Structure and Spectroscopy, Ohio State University, Columbus, Ohio, September 1968.

43. H. M. Pickett, Harvard University, Cambridge, Massachusetts, personal communication.

44. A. H. Brittain, Post Doctor for Professor R. H. Schwendeman in 1969-70; present address: Department of Chemistry, University of Bristol, Bristol, England.

45. R. C. Tolman, Principles of Statistical Mechanics, Oxford University Press, New York, 1930, Chapter IX.

46. T. Oka, J. Chem. Phys., 45, 754 (1966).

47. T. Oka, J. Chem. Phys., 47, 13 (1967).

48. T. Oka, J. Chem. Phys., 47, 4852 (1967).

49. T. Oka, J. Chem. Phys., 48, 4919 (1968).

50. T. Oka, J. Chem. Phys., 49, 3135 (1968).

51. R. M. Lees and T. Oka, J. Chem. Phys., 51, 3027 (1969).

52. C. O. Britt and J. E. Boggs, J. Chem. Phys., 45, 3877 (1966).

53. R. S. Anderson, Phys. Rev., 97, 1654 (1955).

54. C. M. Johnson and D. M. Slager, Phys. Rev., 87, 677 (1952).

55. C. H. Townes, A. N. Holden, and F. R. Merritt, Phys. Rev., 74, 1113 (1948).

56. H. Feeny, H. Lackner, P. Moser, and W. V. Smith, J. Chem. Phys., 22, 79 (1954).

57. A. Dymanus, H. A. Dijkerman, and G. R. D. Zijderveld, J. Chem. Phys., 32, 717 (1960).

58. B. Bleaney and R. P. Penrose, Proc. Roy. Soc., A189, 358 (1947).

59. C. H. Townes, Phys. Rev., 70, 109A, 665 (1946).

60. R. L. Legan, J. A. Roberts, E. A. Rinehart, and C. C. Lin, J. Chem. Phys., 43, 4337 (1965).

61. J. A. Fulford, Nature, 188, 1097 (1960).

APPENDICES

APPENDIX A

DEFINITIONS OF THE FITTING PARAMETERS USED IN THE COMPUTER PROGRAM WBFITP3

The expression for the time dependent absorption coefficient is given by Eq. (6-64). If the definitions

$$\cos^2\phi = \frac{a^2}{a^2 + \Omega^2} , \tag{A-1}$$

$$\sin^2\phi = \frac{\Omega^2}{a^2 + \Omega^2} , \tag{A-2}$$

and $$K = \frac{4\pi\omega N\Delta^o}{c} \tag{A-3}$$

are made, where $a = 1/\tau$, a new expression for Eq. (6-64) can be written as follows:

$$\alpha = K\,|\mu^2|\,[\cos^2\phi - \cos\phi e^{-a(t+t_o)}\cos(\Omega t + t_o)] . \tag{A-4}$$

Eq. (A-4) is related to the signal at the crystal detector by the relation

$$S = S^o - \sum_M \int_d^a \int_o^L \alpha P dx dz , \tag{A-5}$$

where the summation over M is the summation over the degenerate M Stark

components of the energy levels for the transition, and P is the power level of the incident radiation. The integrations over x and z in Eq. (A-5) are a result of the power variation in the sample cell. The integral over x is across the face of the cell and the integral over z is down the length of the cell. The integrations are done numerically. The dependence of μ, ϕ, and Ω is, therefore, changed from dependence on a, z, and summation over M to dependence on k, n, and M, respectively. This leads to the following expression for Eq. (A-5):

$$S = S^{o} - \sum_{M}\sum_{k}\sum_{n} K(\mu_M)^2 \cos^2\phi_{Mkn} P_{kn}$$

$$+ \sum_{M}\sum_{k}\sum_{n} K(\mu_M)^2 P_{kn} \cos\phi_{Mkn} e^{-a(t+t_o)} \cos(\Omega_{Mkn} t + t_o). \qquad \text{(A-6)}$$

In this equation P_{kn} is defined by Eq. (8-2).

The dipole moment contribution is given by the expression

$$\mu_M^2 = \mu_o^2 f_M , \qquad \text{(A-7)}$$

where $$f_M = f(M)^2/f_s \qquad \text{(A-8)}$$

is the M-dependent part of μ_M^2. The constant f_s is defined such that

$$\Sigma f_M = 1. \qquad \text{(A-9)}$$

The f(M) of Eq. (A-8) is related to the relative intensity of the Stark components to each other and f_s is a normalizing factor.

The fitting parameters varied in the computer program WBFITP3 are then defined as follows:

$$v(1) = (P_{kn})^{-1/2} \Omega/f_M , \qquad \text{(A-10)}$$

where $\Omega = \mu_o F^o/\hbar$. (A-11)

$$v(2) = a = 1/\tau . \tag{A-12}$$

$$v(3) = KP^o\mu_o^2 \tag{A-13}$$

and is related to the amplitude of the "wiggles" at time t = 0.

$$v(4) = t_o . \tag{A-14}$$

v(5) is taken to be the steady-state value of the signal S and is time independent. Eq. (A-6) has three terms; the first two are time independent and the third is time dependent. As time increases, i.e., the steady-state appears, the third term vanishes. Therefore, it is apparent that the expression for v(5) is given by the equation

$$v(5) = S^o - \sum_M \sum_k \sum_n K(\mu_M)^2 \cos^2\phi_{Mkn} P_{kn} . \tag{A-5}$$

The expression used for fitting the data can simply be expressed by the following relation

$$S = v(5) + S',$$

where S' is the time dependent term of Eq. (A-6).

APPENDIX B

TABLES OF FINAL FITTING PARAMETERS OBTAINED WITH WBFITP3

The tables on the following pages give a complete listing of the fitting parameters, the experimental pressures and powers, and the S^{o} values for all of the experimental runs used to obtain the results reported in this investigation.

The results of the fittings on the OCS J = 0 → 1 transition using the computer program WBFITP3 are given in Table IX. The results of the fittings on the OCS J = 1 → 2 transition are given in Table X. Table XI gives the results of the fittings on the NH_3 J,K = 3,3 transition.

Table IX. Final Values of the Fitting Parameters Obtained for the OCS J = 0 → 1 Transition.

Run #	V(1)	V(2)	V(3)	V(4)	V(5)	S^o	Press.	Power
1	0.154	3.479	684.	0.130	725.	939.	76.60	51.61
2	0.142	2.386	675.	0.127	745.	867.	52.74	
3	0.144	1.889	623.	0.116	777.	835.	35.62	
4	0.145	1.409	1022.	0.114	811.	858.	22.58	
5	0.144	1.241	827.	0.122	780.	802.	15.88	
6	0.153	1.471	1095.	0.189	814.	912.	32.52	26.52
7	0.152	1.502	540.	0.170	786.	841.	32.84	
8	0.155	1.744	343.	0.157	628.	678.	38.52	
9	0.152	1.721	993.	0.162	782.	920.	38.84	
10	0.155	1.446	945.	0.156	824.	912.	32.80	
11	0.156	1.448	2669.	0.180	1552.	1805.	33.30	
12	0.153	1.845	711.	0.149	763.	877.	41.80	
13	0.155	1.868	717.	0.184	758.	875.	42.43	
14	0.153	1.828	710.	0.171	765.	881.	42.76	
16	0.145	3.116	325.	0.120	613.	743	83.42	51.00
17	0.147	3.345	342.	0.141	609.	745.	83.56	44.88
18	0.151	3.329	340.	0.156	604.	750.	83.64	38.76
19	0.150	3.339	353.	0.158	688.	841.	83.70	32.64
20	0.151	3.575	370.	0.206	628.	790.	83.76	26.52
21	0.152	3.662	379.	0.255	615.	785.	83.72	20.40
25	0.154	2.667	675.	0.239	746.	886.	57.42	51.00
26	0.143	2.372	708.	0.110	683.	836.	57.76	44.88

continued

Table IX (cont'd.)

Run #	V(1)	V(2)	V(3)	V(4)	V(5)	S^{o}	Press.	Power
27	0.151	2.546	715.	0.165	694.	856.	57.95	38.76
28	0.149	2.547	735.	0.161	706.	871.	58.15	32.64
29	0.151	2.447	711.	0.160	694.	874.	58.31	26.52
30	0.151	2.535	697.	0.227	692.	840.	58.46	20.40
32	0.149	2.342	587.	0.385	626.	854.	58.80	10.20
36	0.159	2.332	652.	0.153	679.	782.	49.30	44.00
37	0.156	2.256	675.	0.174	749.	860.	47.82	38.76
38	0.153	2.222	696.	0.293	713.	834.	49.25	32.64
39	0.144	1.869	706.	0.386	717.	826.	43.43	26.52
40	0.150	1.857	655.	0.366	798.	918.	44.12	20.40
42	0.160	1.782	582.	0.266	739.	882.	44.71	10.20
44	0.153	2.003	464.	0.581	669.	831.	45.08	5.10
46	0.153	1.058	954.	0.165	772.	797.	16.52	44.88
47	0.152	1.020	1006.	0.208	806.	833.	16.86	38.76
48	0.153	0.987	1041.	0.247	931.	963.	17.10	32.64
49	0.151	0.952	1052.	0.301	769.	807.	17.36	26.52
50	0.150	0.854	1055.	0.316	823.	864.	16.93	20.40
51	0.153	0.777	1013.	0.264	830.	880.	17.41	15.30
52	0.151	0.681	934.	0.289	834.	890.	17.60	10.20
53	0.153	0.667	701.	0.319	746.	824.	17.70	5.10
59	0.154	1.614	1268.	0.269	797.	913.	35.40	32.64
60	0.154	1.532	1256.	0.264	826.	953.	35.50	26.52
61	0.154	1.531	1217.	0.237	792.	939.	35.60	20.40

continued

Table IX (cont'd.)

Run #	V(1)	V(2)	V(3)	V(4)	V(5)	S^o	Press.	Power
62	0.157	1.457	1113.	0.233	750.	914.	35.75	15.30
63	0.158	1.385	970.	0.308	716.	905.	36.04	10.20
84	0.145	1.442	1164.	0.142	799.	860.	25.06	51.00
85	0.151	1.366	1252	0.129	829.	900.	25.78	44.88
86	0.154	1.231	1283.	0.178	793.	861.	24.44	38.76
87	0.153	1.194	1289.	0.182	753.	851.	25.20	32.64
88	0.155	1.198	1282.	0.166	762.	847.	25.82	26.52
89	0.155	1.141	1286.	0.218	789.	890.	24.80	20.40
90	0.156	1.064	1214.	0.232	800.	902.	26.44	15.50
92	0.159	0.915	830.	0.586	740.	868.	22.28	5.10

Table X. Final Values of the Fitting Parameters Obtained for the OCS J = 1 → 2 Transition.

Run #	V(1)	V(2)	V(3)	V(4)	V(5)	S^o	Press.	Power
1T	0.0586	1.695	2110.	0.279	378.	647.	35.18	38.73
2T	0.0583	1.669	2084.	0.315	371.	654.		34.58
3T	0.0617	1.618	2029.	0.266	363.	662.		30.43
4T	0.0618	1.543	2042	0.284	355.	663.		26.28
5T	0.0615	1.523	1938.	0.306	341.	674.		22.13
6T	0.0622	1.457	1841.	0.400	329.	686.		17.98
7T	0.0629	1.439	1683.	0.476	310.	702.		13.83
8T	0.0635	1.416	1485.	0.560	288.	715.		9.68
9T	0.0616	1.580	2037.	0.239	456.	652.	29.28	38.73
10T	0.0620	1.550	2003.	0.332	450.	659.		34.58
11T	0.0617	1.511	1990.	0.341	444.	656.		30.43
12T	0.0621	1.327	1906.	0.340	311.	554.		26.28
13T	0.0621	1.291	1847.	0.336	301.	561.		22.13
14T	0.0632	1.256	1732.	0.397	291.	574.		17.98
15T	0.0654	1.186	1590	0.465	281.	580.		13.83
16T	0.0649	1.242	1443.	0.625	259.	598.		9.68
17T	0.0620	1.207	1902.	0.250	358.	504.	24.86	38.73
18T	0.0589	1.297	2038.	0.557	355.	508.		34.58
19T	0.0609	1.203	1905.	0.358	352.	512.		30.43
20T	0.0611	1.152	1874.	0.345	346.	519.		26.28
21T	0.0616	1.118	1817.	0.340	340.	527.		22.13

continued

Table X (cont'd.)

Run #	V(1)	V(2)	V(3)	V(4)	V(5)	S^o	Press.	Power
22T	0.0622	1.083	1727.	0.391	331.	535.		17.98
23T	0.0636	1.043	1595.	0.463	321.	545.		13.83
24T	0.0638	1.024	1411.	0.572	302.	560.		9.68
25T	0.0610	1.120	1790.	0.255	385.	476.	20.12	38.73
26T	0.0611	1.089	1784.	0.255	382.	479.		34.58
27T	0.0613	0.978	1845.	0.277	379.	489.		30.43
28T	0.0610	0.944	1822.	0.361	376.	491.		26.28
29T	0.0614	0.925	1762.	0.352	372.	496.		22.13
30T	0.0620	0.899	1680.	0.402	366.	504.		17.98
31T	0.0628	0.875	1571.	0.459	357.	514.		13.83
32T	0.0643	0.882	1399.	0.623	345.	525.	20.12	9.68
33T	0.0611	0.979	1553.	0.221	405.	452.	15.05	38.73
34T	0.0618	0.779	1605.	0.305	400.	459.		34.58
35T	0.0638	0.728	1652.	0.287	401.	457.		30.43
36T	0.0609	0.796	1612.	0.298	401.	462.		26.28
37T	0.0613	0.752	1605.	0.364	398.	469.		22.13
38T	0.0622	0.718	1568.	0.415	396.	472.		17.98
39T	0.0631	0.693	1482.	0.465	391.	479.		13.83
40T	0.0654	0.704	1336.	0.628	385.	488.		9.68

Table XI. Final Values of the Fitting Parameters Obtained for the NH_3 J,K = 3,3 Transition.

Run #	V(1)	V(2)	V(3)	V(4)	V(5)	S^o	Press.	Power
67T	0.1063	4.802	974.	0.127	310.	533.	22.00	34.58
68T	0.1070	4.400	929.	0.140	309.	534.	21.50	30.43
69T	0.1070	4.206	898.	0.154	305.	538.	21.38	26.28
70T	0.1076	3.952	848.	0.176	300.	542.	21.34	22.13
71T	0.1092	3.859	788.	0.184	295.	546.	21.30	17.98
72T	0.1101	3.634	693.	0.238	288.	551.	21.00	13.83
73T	0.1144	3.380	563.	0.251	280.	556.	21.00	9.68
74T	0.1062	3.844	899.	0.139	344.	505.	18.00	34.58
75T	0.1073	3.542	873.	0.139	342.	507.	18.00	30.43
76T	0.1073	3.190	847.	0.159	338.	510.	17.90	26.28
77T	0.1069	3.189	858.	0.176	333.	516.	17.84	22.13
78T	0.1087	3.174	798.	0.198	327.	520.	17.82	17.98
79T	0.1108	3.081	729.	0.207	321.	525.	17.76	13.83
80T	0.1150	3.018	627.	0.249	312.	532.	17.70	9.68
81T	0.1047	3.155	870.	0.142	371.	483.	14.60	34.58
82T	0.1057	2.881	865.	0.144	368.	486.	14.68	30.43
83T	0.1066	2.606	850.	0.152	365.	489.	14.68	26.28
84T	0.1080	2.473	816.	0.174	362.	492.	14.68	22.13
85T	0.1097	2.534	360.	0.189	357.	496.	14.66	17.98
86T	0.1121	2.460	693.	0.204	351.	500.	14.66	13.83
87T	0.1154	2.450	666.	0.245	342.	509.	14.66	9.68

continued

Table XI (cont'd.)

Run #	V(1)	V(2)	V(3)	V(4)	V(5)	S^{o}	Press.	Power
88T	0.1029	2.595	2097.	0.143	339.	525.	11.40	34.58
89T	0.1033	2.254	2157.	0.151	334.	530.	11.55	30.43
90T	0.1050	2.039	2185.	0.155	328.	536.	11.62	26.28
91T	0.1065	1.974	2134.	0.176	321.	544.	11.64	22.13
92T	0.1093	1.999	2013.	0.187	311.	552.	11.70	17.98
93T	0.1120	2.005	1874.	0.207	299.	563.	11.70	13.83
94T	0.1160	1.970	1662.	0.243	281.	576.	11.74	9.68
95T	0.1011	2.153	2006.	0.149	375.	492.	8.72	34.58
96T	0.1014	1.797	2145.	0.163	372.	496.	8.86	30.43
97T	0.1040	1.594	2239.	0.163	368.	502.	8.96	26.28
98T	0.1062	1.560	2198.	0.180	363.	507.	9.08	22.13
99T	0.1091	1.617	2074.	0.183	356.	514.	9.18	17.98
100T	0.1119	1.630	1948.	0.207	347.	523.	9.22	13.83
101T	0.1169	1.598	1788.	0.245	345.	533.	9.28	9.68